ELSEVIER

Contents lists available at ScienceDirect

# Construction and Building Materials

journal homepage: www.elsevier.com/locate/conbuildmat





# Modeling mixing kinetics for large-scale production of Ultra-High-Performance Concrete: effects of temperature, volume, and mixing method

Jiang Du<sup>a</sup>, Soroush Mahjoubi<sup>a</sup>, Yi Bao<sup>a</sup>, Nemkumar Banthia<sup>b</sup>, Weina Meng<sup>a,\*</sup>

#### ARTICLE INFO

Keywords:
Mixing kinetics
Mixing temperature
Mixing torque
Mixing volume
Multi-batching method
Ultra-high-performance concrete (UHPC)

#### ABSTRACT

The mixing of ultra-high-performance concrete (UHPC) featuring low water-to-binder ratios involves different evolution of microstructures and mixing torques from conventional concrete. This paper investigates the mixing kinetics of UHPC in the mixing process, presents a mixing kinetics model to predict the mixing torque at an arbitrary time instant, and develops a multi-batching method to reduce the mixing torque for large-volume production of UHPC. The presented mixing kinetics model considers the effects of mixing temperature, mixing volume, and mixing methods. The mixing kinetics model is calibrated using experimental data, and the calibrated model shows high prediction accuracy. The multi-batching method enables large-volume mixing of UHPC by reducing the mixing torque while retaining desired flowability and hardened properties of UHPC. Specifically, when the number of sub-batches is two, the peak mixing torque of the multi-batching method was approximately reduced to half of the peak mixing torque of the mono-batching method. Besides, the differences in workability, compressive strength, and autogenous shrinkage by using the multi-batching method and mono-batching method are within 5%. Finally, the reliability and repeatability of the presented mixing kinetics model are verified through the validation tests with different UHPC mixture designs and mixing methods. This study will advance understandings of the mixing kinetics for UHPC and promote large-volume UHPC production.

#### 1. Introduction

Ultra-high-performance concrete (UHPC) is a group of advanced cementitious composites with self-consolidating property, high mechanical properties, and excellent durability due to the dense microstructures [1–7]. The dense microstructures are generated by the unique mixture design of UHPC with a low water-to-binder ratio (w/b < 0.25) and high packing density [8–10]. Appropriate incorporation of chopped fibers is capable of imparting strain-hardening property and high tensile strength [11]. Due to its exceptional properties, UHPC attracts increasing interest in engineering applications, such as precast girders and piles [12–14], cast-in-place connections and joints [15–18], jackets for columns [19], bridge deck overlay [20–23], bridge maintenaice [24–26], and railway applications [27,28]. UHPC improved the mechanical performance and durability of structures, facilitated construction, and enabled aesthetically appealing designs of structures. To reduce the upfront cost, cost-effective UHPC mixtures were developed

by using locally available materials and industrial by-products [29–32]. For instance, Meng et al. [32] proposed mixtures that reduced the unit cost of UHPC by 70%, while retaining the high mechanical properties and durability, through incorporating supplementary cementitious materials and natural river sand. Development of cost-effective UHPC promoted acceptance of UHPC in structural applications.

Currently, one of the major challenges in structural applications of UHPC is the large-volume production of UHPC [33]. When the volume of UHPC is increased, it becomes difficult to mix the ingredients using normal mixers because the demand of mixing torque exceeds the torque capacity of the mixers [34]. Previous studies proposed that the high demand of mixing torque was attributed to the high plastic viscosity of UHPC [35–38], so scholars attempted to reduce the plastic viscosity of UHPC by modifying the mixture design or adding chemical admixtures. However, reducing the plastic viscosity of UHPC compromised the mechanical properties and durability because recent research found that adequate viscosity was essential to ensure appropriate dispersion and

E-mail address: wmeng3@stevens.edu (W. Meng).

a Department of Civil, Environmental and Ocean Engineering, Stevens Institute of Technology, Hoboken, NJ, USA

b Department of Civil Engineering, The University of British Columbia, Vancouver, BC V6T 1Z4, Canada

<sup>\*</sup> Corresponding author.

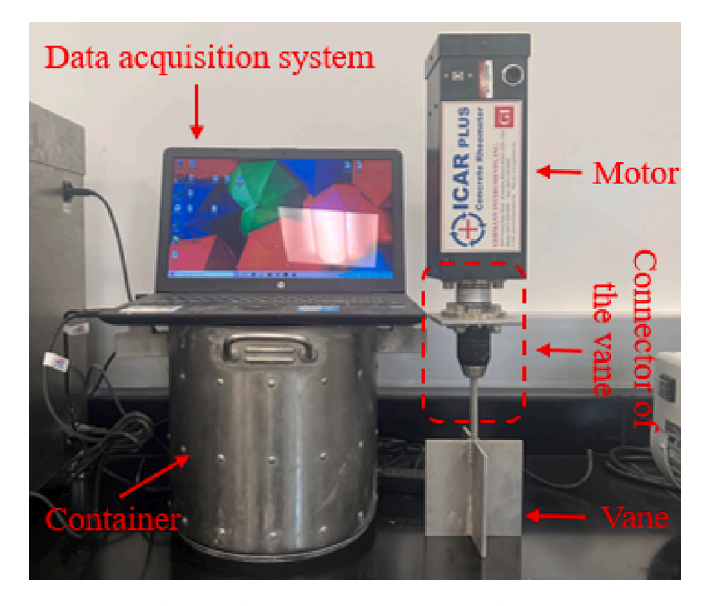
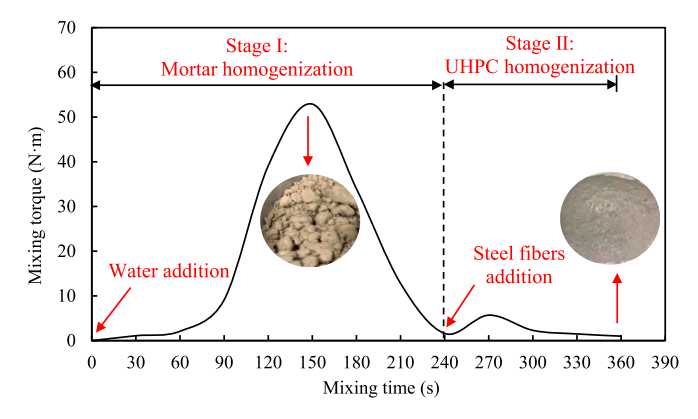


Fig. 1. The ICAR rheometer for measurement of mixing torque.



 $\textbf{Fig. 2.} \ \ \textbf{Mixing torque versus mixing time curve of UHPC production process.}$ 

orientation of chopped fibers and prevent segregation of sand in UHPC [36,38]. More importantly, the high demand of mixing torque was also related to the turnover phase when the heterogeneous UHPC transformed from the dry powder to the homogenous UHPC mortar [33]. Therefore, some engineers employed high-intensity mixers with high torque capacity to overcome the demand of mixing torque [39,40], but the price of the high energy mixer is approximately 20 times higher than the normal pan mixer. For the cast-in-place projects on the job sites, the high cost limits the promotion of UHPC mixtures. In addition, it was unknown whether use of high-intensity mixers compromised the fresh and hardened properties of UHPC due to overheat. Intensive heat release was found in mixing of UHPC using normal mixers [33], and the heat release was exacerbated by using high-intensity mixers. In short, large-volume production of UHPC is still a challenge.

Subsequently, to address the existing challenge, scholars proposed to reduce the mixing torque by modifying the mixing procedures. In normal mixing of UHPC, binder is mixed with sand before mixing water is introduced. Sand is capable of perturbing agglomeration of binder and homogenizing the binder-sand system. Agglomeration of binder compromises the mechanical properties and durability. In reference [33], scholars proposed to introduce sand after binder and water were mixed. In reference [41], scholars divided the binder into two portions and respectively mixed them with water and sand. It remains unknown whether agglomeration of binder occurred and affected the key properties of the mixtures in the above attempts. Also, it is unclear how much

mixing torque was reduced and how the mixing process was designed. The unknown information is associated with fundamental knowledge gaps on the mixing kinetics of UHPC.

The mixing kinetics of conventional concrete (CC) and selfcompacting concrete (SCC) were elaborated in references [42-44]. The mixing process was divided into multiple stages involving different material behaviors and mixing phenomena, as stated in references [42,43]. A mixing kinetics model was developed to describe evolution of mixing power in five successive stages in mixing CC and/or SCC [44]. The five stages were designated to be (i) dry powder stage, (ii) dry granule stage, (iii) wet granule stage, (iv) granular suspension stage, and (v) dispersed granular stage, which were characterized by different microstructures. The proposed mixing kinetics model consisted of four phases, respectively designated as (i) granule growth, (ii) granule coalescence, (iii) granule dissolution, and (iv) agglomerate dispersion. It was suggested using mixing power to identify transient stages in mixing concrete. To date, there is lack of knowledge on the mixing kinetics of UHPC. It is unknown whether the mixing kinetics of conventional concrete and SCC is the same with UHPC due to the extremely low w/b, and it is unclear how the high mixing torque in production of UHPC can be effectively reduced. The following questions are vet to be answered: (1) How does the mixing torque evolve in the mixing of UHPC? (2) What are the main factors that affect the evolution of mixing torque of UHPC? (3) How does the mixing procedure affect the evolution of mixing torque of UHPC? (4) How the mixing procedure can be designed to reduce the mixing torque?

To answer the above questions, this research investigates the mixing kinetics of UHPC and presents a mixing kinetics model to guide the design of mixing process for large-volume production of UHPC. This research has four objectives: (1) to evaluate the effects of mixing temperature, mixing volume, and mixing method on the mixing torque evolution; (2) to understand the mechanism of the evolution of the mixing torque for UHPC mixtures; (3) to develop a mathematical mixing kinetics model to quantify the evolution of the mixing torque; and (4) to develop a method to design and optimize the mixing protocol for largevolume production of UHPC. This research has four novelties: (1) The mixing kinetics of UHPC is revealed for the first time. Different from conventional concrete, the consolidation and growth stages for UHPC can only depend on the squeezed water from particles, which significantly increases the peak mixing torque. (2) The key impact factors for the mixing kinetics of UHPC include mixing temperature, mixing volume, and mixing method. (3) The presented multi-batching method significantly reduces the peak mixing torque of UHPC without significantly reducing mixing efficiency and key properties of UHPC. (4) A mathematical mixing kinetics model is proposed for the first time to quantify the mixing torque evolution for UHPC mixtures ( $R^2 \ge 95\%$ ). To achieve the objectives, comprehensive laboratory experiments were conducted and four UHPC mixtures and two mixing methods were applied to develop, evaluate, and validate the mixing kinetics model. To achieve the objectives, comprehensive laboratory experiments were conducted and four UHPC mixtures and two mixing methods were applied to develop, evaluate, and validate the mixing kinetics model. This research advances knowledge on the mixing kinetics of UHPC and facilitates large-volume production of UHPC for industrial applications.

# 2. Experimental investigations on mixing kinetics

#### 2.1. Quantitative evaluation of mixing torque

The mixing torque of UHPC mixtures was measured using a rheometer (model: ICAR Plus), shown in Fig. 1. The container of the rheometer measured 280 mm in diameter and height. The vane of the rheometer measured 127 mm in diameter and height.

The mixing torque evolution of the whole mixing process for UHPC production was investigated. For each mixture, the mixing torque was recorded every 30 s starting from water addition, until the mixing torque

**Table 1**Chemical and physical properties of raw materials.

Property	Type I cement	GGBFS	Silica fume	River sand
SiO <sub>2</sub> (%)	22.44	36.21	95.5	80.3
Al <sub>2</sub> O <sub>3</sub> (%)	2.76	11.1	0.7	10.5
Fe <sub>2</sub> O <sub>3</sub> (%)	2.24	0.76	0.3	3.43
CaO (%)	68.05	43.75	0.4	1.72
MgO (%)	0.91	5.09	0.5	1.70
SO <sub>3</sub> (%)	2.25	2.21	-	1.07
Na <sub>2</sub> O (%)	0.19	0.23	0.4	_
K <sub>2</sub> O (%)	0.11	0.40	-	_
TiO <sub>2</sub> (%)	0.14	0.58	-	_
P <sub>2</sub> O <sub>5</sub> (%)	0.09	0.02	-	_
Mn <sub>2</sub> O <sub>3</sub> (%)	0.03	0.36	-	_
C <sub>3</sub> S (%)	62.35	_	_	-
C <sub>2</sub> S (%)	20.28	_	-	_
C <sub>3</sub> A (%)	1.42	_	-	_
C <sub>4</sub> AF (%)	5.83	_	-	_
Loss on ignition (%)	1.28	0.72	2.6	1.28
Specific gravity, SSD	3.15	2.9	2.20	2.65

stabilized. Fig. 2 plots the representative curve of mixing torque versus mixing time of a UHPC mixture, reflecting the mixing torque evolution process. Results indicated that the dramatic increment of the mixing torque during the UHPC production process was mainly happened in Stage I (i.e., mortar homogenization process). Afterwards, the addition of steel fibers in Stage II (i.e., UHPC homogenization process) had negligible contribution on the evolution of the mixing torque. Therefore, in this study, the discussion about the mixing kinetics of UHPC was focusing on the mortar homogenization process.

# **Table 2** Mixture design (kg/m<sup>3</sup>).

Code	Cement	GGBFS	Silica fume	Sand	HRWR	VMA	Water	Steel fiber
M1	468.2	646.7	0	985.1	11.4	0	249.2	156
M2	468.2	646.7	0	985.1	11.4	10.9	238.1	156
M3	468.2	646.7	0	985.1	11.4	21.9	227.3	156
M4	1049.0	0	81.4	980.5	23.2	0	244.8	156

All (Water + HRWR)

#### 2.2. Raw materials

The investigated mixtures were composed of binders, fine aggregates, water, chemical admixtures, and steel fibers. The binder was composed of Type I Portland cement, silica fume, and GGBFS from a local plant in New Jersey. River sand was used as fine aggregates. The chemical compositions of the binder and fine aggregates were characterized by X-ray fluorescence, as listed in Table 1. To improve workability, a polycarboxylate-based high-range water reducer (HRWR) was used. The solid content and specific gravity of HRWR were 34.4% and 1.05, respectively. A viscosity-modifying admixture (VMA) was used to adjust viscosity. The VMA was a ready-to-use product (BASF Master-Matrix VMA 362), with a water content of 95% and a specific density of 1.002. Straight steel fibers measured 0.2 mm in diameter and 13 mm in length were incorporated. The tensile strength and elasticity modulus of steel fibers are 1.9 GPa and 203 GPa.

#### 2.3. Mixture design

Four different UHPC mixtures, listed in Table 2, were investigated in this study. M1 is a representative cost-effective UHPC mixture developed in prior research by the authors [27]. The binder consisted of 40% cement and 60% GGBFS by volume. M2 and M3 had the same binder system but the VMA contents increased from 1% to 2% by mass of binder, to investigate the effect of viscosity on mixing kinetics. The binder-to-sand ratio was 1:1 by volume. The water-to-binder ratio was 0.23 by mass. M4 had a different binder system from mixtures M1 to M3. In mixture M4, the binder was composed of 90% cement and 10% silica fume by volume. The b/s and w/b were the same with mixtures M1 to

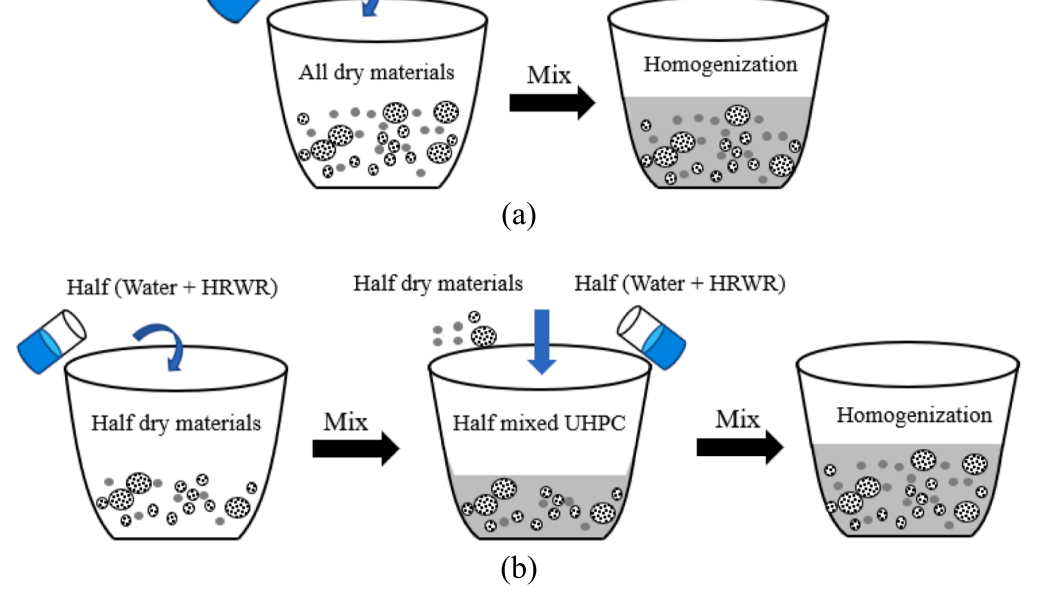


Fig. 3. Illustration of mixing methods: (a) mono-batching method; and (b) multi-batching method.

**Table 3** Investigated mixing cases.

Case	Designation code	UHPC Mixture	Volume (Liters)	Temperature (°C)	Addition time (second
Model	development				
C1	M1-1.5-10C	M1	1.5	10	0
C2	M1-1.5-20C	M1	1.5	20	0
C3	M1-1.5-30C	M1	1.5	30	0
C4	M1-3.0-10C	M1	3.0	10	0
C5	M1-3.0-20C	M1	3.0	20	0
C6	M1-3.0-30C	M1	3.0	30	0
C7	M1-4.5-10C	M1	4.5	10	0
C8	M1-4.5-20C	M1	4.5	20	0
C9	M1-4.5-30C	M1	4.5	30	0
C10	M1-6.0-10C	M1	6.0	10	0
C11	M1-6.0-20C	M1	6.0	20	0
C12	M1-6.0-30C	M1	6.0	30	0
C12	M1-1.5-1.5	M1	3.0	10	0, 30
	(30)-10C				
C14	M1-1.5–1.5 (60)-10C	M1	3.0	10	0, 60
C15	M1-1.5–1.5 (75)-10C	M1	3.0	10	0, 75
C16	M1-1.5–1.5 (90)-10C	M1	3.0	10	0, 90
C17	M1-1.5–1.5 (105)-10C	M1	3.0	10	0, 105
C18	M1-1.5–1.5 (120)-10C	M1	3.0	10	0, 120
C19	M1-1.5-1.5	M1	3.0	10	0, 150
C20	(150)-10C M1-1.5–1.5	M1	3.0	10	0, 180
C21	(180)-10C M1-1.5–1.5	M1	3.0	20	0, 30
C22	(30)-20C M1-1.5–1.5	M1	3.0	20	0, 60
C23	(60)-20C M1-1.5–1.5	M1	3.0	20	0, 75
C24	(75)-20C M1-1.5–1.5	M1	3.0	20	0, 90
C25	(90)-20C M1-1.5–1.5	M1	3.0	20	0, 105
C26	(105)-20C M1-1.5–1.5	M1	3.0	20	0, 120
C27	(120)-20C M1-1.5–1.5	M1	3.0	20	0, 150
C28	(150)-20C M1-1.5–1.5	M1	3.0	20	0, 180
C29	(180)-20C M1-1.5–1.5	M1	3.0	30	0, 30
C30	(30)-30C M1-1.5–1.5	M1	3.0	30	0, 60
C31	(60)-30C M1-1.5–1.5	M1	3.0	30	0, 75
C32	(75)-30C M1-1.5-1.5	M1	3.0	30	0, 90
C33	(90)-30C M1-1.5-1.5	M1	3.0	30	0, 105
C34	(105)-30C M1-1.5–1.5	M1	3.0	30	0, 120
	(120)-30C				
C35	M1-1.5–1.5 (150)-30C	M1	3.0	30	0, 150
C36	M1-1.5–1.5 (180)-30C	M1	3.0	30	0, 180
	validation				
C37	M2-3.0-20C	M2	3.0	20	0
C38	M3-3.0-20C	М3	3.0	20	0
C39	M4-3.0-20C	M4	3.0	20	0
C40	M2-1.5-1.5	M2	3.0	20	0, 150
	(150)-20C				
C41	M3-1.5-1.5 (150)-20C	М3	3.0	20	0, 150
C42	M4-1.5–1.5 (150)-20C	M4	3.0	20	0, 150

Table 3 (continued)

Case	Designation code	UHPC Mixture	Volume (Liters)	Temperature (°C)	Addition time (seconds)
C43	M2-1.5-1.5 (180)-20C	M2	3.0	20	0, 180
C44	M3-1.5-1.5 (180)-20C	М3	3.0	20	0, 180
C45	M4-1.5-1.5 (180)-20C	M4	3.0	20	0, 180
C46	M1-1.0-1.0 (180)-1.0(195)- 20C	M1	3.0	20	0, 180, 195
C47	M1-1.0-1.0 (180)-1.0(210)- 20C	M1	3.0	20	0, 180, 210
C48	M1-1.0-1.0 (180)-1.0(240)- 20C	M1	3.0	20	0, 180, 240
C49	M1-1.0-1.0 (180)-1.0(270)- 20C	M1	3.0	20	0, 180, 270

М3.

# 2.4. Mixing variables

The large-volume UHPC production on job sites still faces challenges: (1) the elevated temperatures during the mixing have negative effects on the workability of fresh UHPC [18]; (2) the mixing capacity of the normal pan mixer limited the allowable mixing volume for large-scale production [19]; (3) the mixing procedures in the lab are not applicable for large-volume UHPC production [16]. Therefore, three key impact factors (i.e., mixing temperature, mixing volume, and mixing procedures) on the mixing kinetics of UHPC were investigated in this study.

# 2.4.1. Mixing temperature

Three different temperature levels were considered in this study, which are 10  $^{\circ}$ C, 20  $^{\circ}$ C, and 30  $^{\circ}$ C, simulating field production of UHPC at different seasons. For each temperature, the raw materials, and apparatuses in direct contact with mixtures, such as the mixing bowl and paddle, were stored in an environmental chamber for 5 h before the mixing to ensure the starting temperature of the mixture is consistent with the target temperature. In addition, the temperature increases during the mixing process is negligible.

# 2.4.2. Mixing volume

Four mixing volumes were considered in this study, which are  $1.5\,L$ ,  $3.0\,L$ ,  $4.5\,L$ , and  $6.0\,L$ . In general, higher mixing volume for each batch is preferred which leads to higher UHPC production efficiency and shorter construction time for UHPC infrastructure.

# 2.4.3. Mixing procedure

A mortar mixer (Hobart® HL-200) with the output capacity of  $11.5\,L$  was used to mix raw materials for production of UHPC in this study. The technical information of the mixer was shown in Table A1 in Appendix. Two types of methods, designated as mono-batching and multibatching, were considered. The mono-batching method represents a normal method for mixing UHPC, with the following steps: (1) to mix binder and sand; (2) to add mixing water and HRWR; and (3) to add steel fibers. In each step, the added ingredients are fully homogenized, as illustrated in Fig. 3(a). The multi-batching method represents an innovative method that involves more steps. To reduce the mixing torque, the binder and sand are divided into multiple portions after they are homogenized, as illustrated in Fig. 3(b).

The two-batching method was set as an example to clarify the multibatching method. The total UHPC mixture was equally divided into two

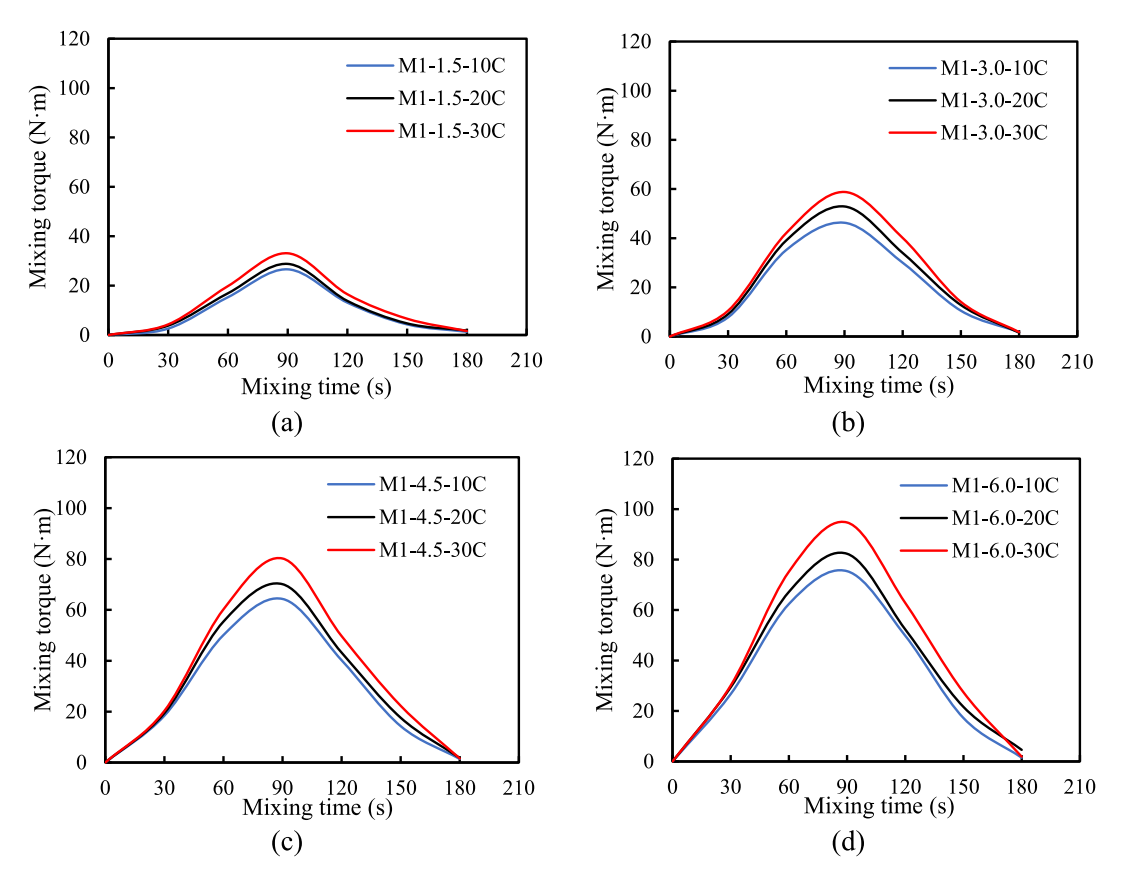


Fig. 4. Results of mixing torque versus mixing time: (a) 1.5 L; (b) 3.0 L; (c) 4.5 L; and (d) 6.0 L.

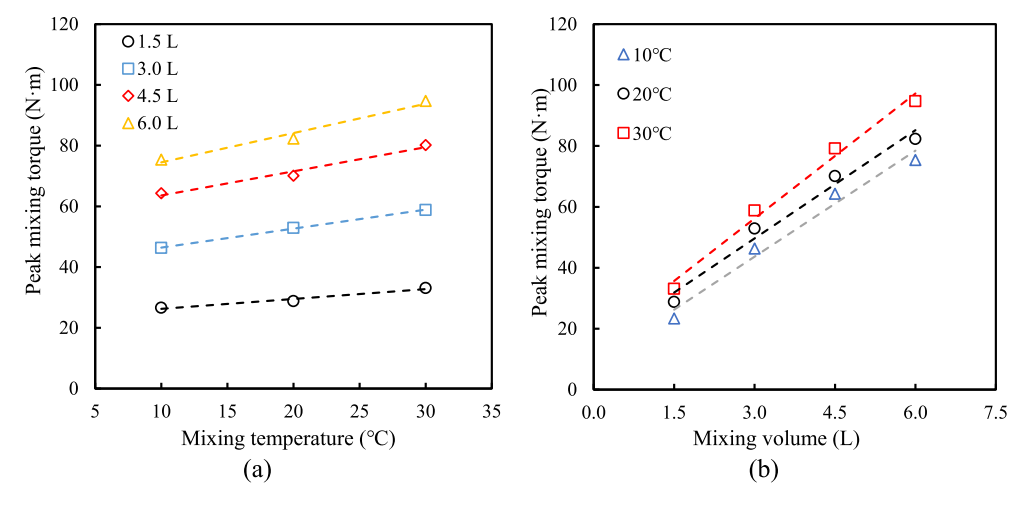


Fig. 5. Regression analysis results of the peak mixing torque  $(Q_{\text{max}})$ : (a) with the mixing temperature (T); and (b) with the mixing volume (V).

sub-batches: (1) 1st sub-batch (50% of the total mass) and (2) 2nd sub-batch (50% of the total mass). In summary, the mixing process consists of four steps: (1) to mix binder and sand; (2) to take a half of mixed binder and sand and add a half of mixing water and HRWR; (3) to add the other half of binder, sand, water, and HRWR; and (4) to add steel fibers. For the multi-batching method, it was identified that the time interval for the addition of the second half portion of ingredients was an important parameter. This study considered eight time intervals, which were  $30 \, \text{s}$ ,  $60 \, \text{s}$ ,  $75 \, \text{s}$ ,  $90 \, \text{s}$ ,  $105 \, \text{s}$ ,  $120 \, \text{s}$ ,  $150 \, \text{s}$ , and  $180 \, \text{s}$ .

# 2.4.4. Investigated cases

Table 3 lists the investigated cases. A total of 49 cases were designed

and tested, designated as C1 to C49. Cases C1 to C36 were designed to develop the mixing kinetic model. Cases C37 to C49 were designed to validate the model. For model development, C1 to C12 represented mono-batching cases, and C13 to C36 represented two-batching cases. For model validation, C37 to C39 represented mono-batching cases, C40 to C45 represented two-batching cases, and C47 to C49 represented three-batching cases. Designation of cases is explained using three cases for example: (1) In case M1-1.5-10C, M1 is the mixture; 1.5 refers to the mixing volume 1.5 L, added at time zero; and 10C refers to mixing temperature 10 °C. (2) In case M1-1.5-1.5(30)-10C, M1 is the mixture; 1.5 refers to the mixing volume of the first sub-batch added at time zero; 1.5(30) refers to the mixing volume of the second sub-batch, added at

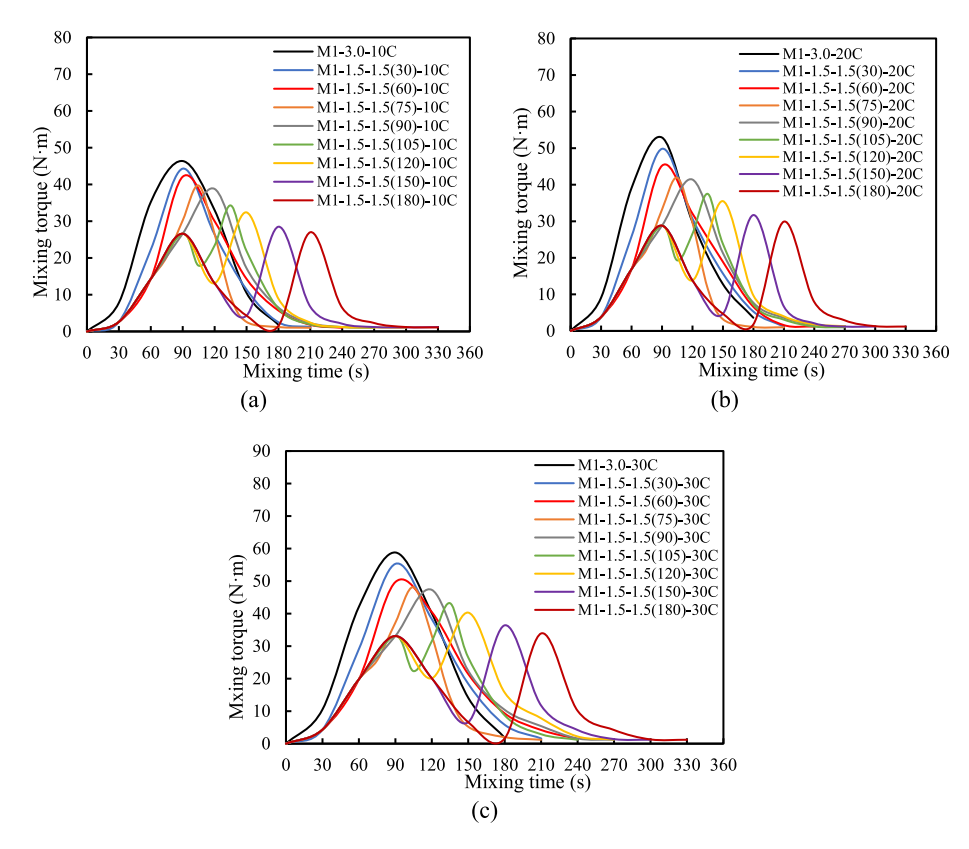


Fig. 6. Mixing torque-time curves affected by mixing methods: (a) 10  $^{\circ}$ C; (b) 20  $^{\circ}$ C; and (c) 30  $^{\circ}$ C.

30 s; and 10C refers to the mixing temperature. (3) In case M1-1.0–1.0 (180)-1.0(195)-20C, 1.0 refers to the mixing volume of the first subbatch; 1.0(180) refers to the mixing volume of the second sub-batch added at 180 s; 1.0(195) refers to the mixing volume of the third subbatch added at 195 s; and 20C is the mixing temperature. The time interval between the second and third sub-batches is 15 s (=195–180).

# 3. Experimental results and discussions on mixing kinetics

This section presents the experimental results of the mixing torque of the UHPC mixtures and discussions on the underlying mechanisms of the evolution of mixing torque. The discussions of the underlying mechanisms focus on the development of microstructures in the mixing process of the powder and liquid phases.

# 3.1. Effects of mixing temperature and mixing volume

Fig. 4 plots the mixing torque versus mixing time for the monobatching cases of mixture M1. The plotted curves reflect the evolution of the mixing torque throughout the mixing process. The different curves correspond to different mixing temperatures and mixing volumes. The comparison of the different curves reveals the effects of mixing temperature and mixing volume on the evolution of the mixing torque. For each mixing volume, the torque-time curves corresponding to different mixing temperatures showed consistent trends. As the mixing time was increased, the mixing torque first increased and then decreased. The peak mixing torque of the different curves corresponded to the mixing time  $t=90~\rm s$ . As the mixing temperature increased from 10 °C to 30 °C, or as the mixing volume increased from 1.5 L to 6.0 L, the peak mixing torque was monotonically increased. By comparing the peak mixing torques corresponding to different temperatures, it was found that the peak mixing torque also increased with the mixing temperature.

To further investigate the effects of mixing temperature and mixing volume on the peak mixing torque, linear regression analysis was

performed. Fig. 5(a) plots the relationship between the peak mixing torque and the mixing temperature for different mixing volumes. For each mixing volume, a straight line was performed to fit the data points. Fig. 5(b) plots the relationship between the peak mixing torque and mixing volume for different temperatures. For each temperature, a straight line was used to fit the data points. In summary, the peak mixing torque approximately linearly increased with the mixing temperature and mixing volume. The slopes of the fitting lines represented the increasing rate of the peak mixing torque with the mixing temperature or mixing volume. For instance, as the mixing volume increased from 1.5 L to 6.0 L, the increasing rate of the peak mixing torque was 197%. As the mixing temperature increased from 10 °C to 30 °C, the increasing rate of the peak mixing torque was 18%. The results revealed the peak mixing volume was more sensitive to the mixing volume than the mixing temperature in the investigated ranges.

# 3.2. Effects of mixing method and time interval

Fig. 6 shows the evolution of mixing torque with different mixing methods and time intervals for mixing of mixture M1 with a total volume of 3 L. The results show consistent phenomena at the different temperatures: (1) When the interval time of the multi-batching method was longer than 90 s, two peaks of mixing torque were generated, corresponding to two sub-batches. (2) For the two peaks, the first peak did not change with the interval time, while the magnitude of the second peak decreased with the increase of the interval time and became stabilized as the interval time reached 150 s. (3) The second peak had a higher magnitude than the first peak, but as the interval increased, the second peak stabilized to the magnitude of the first peak. (4) The peak mixing torque of the mono-batching method was higher than that of the multi-batching method.

In the multi-batching method, the total torque at an arbitrary time instant is equal to the sum of the torques associated with the different sub-batches, meaning that the evolution curve of the total mixing torque

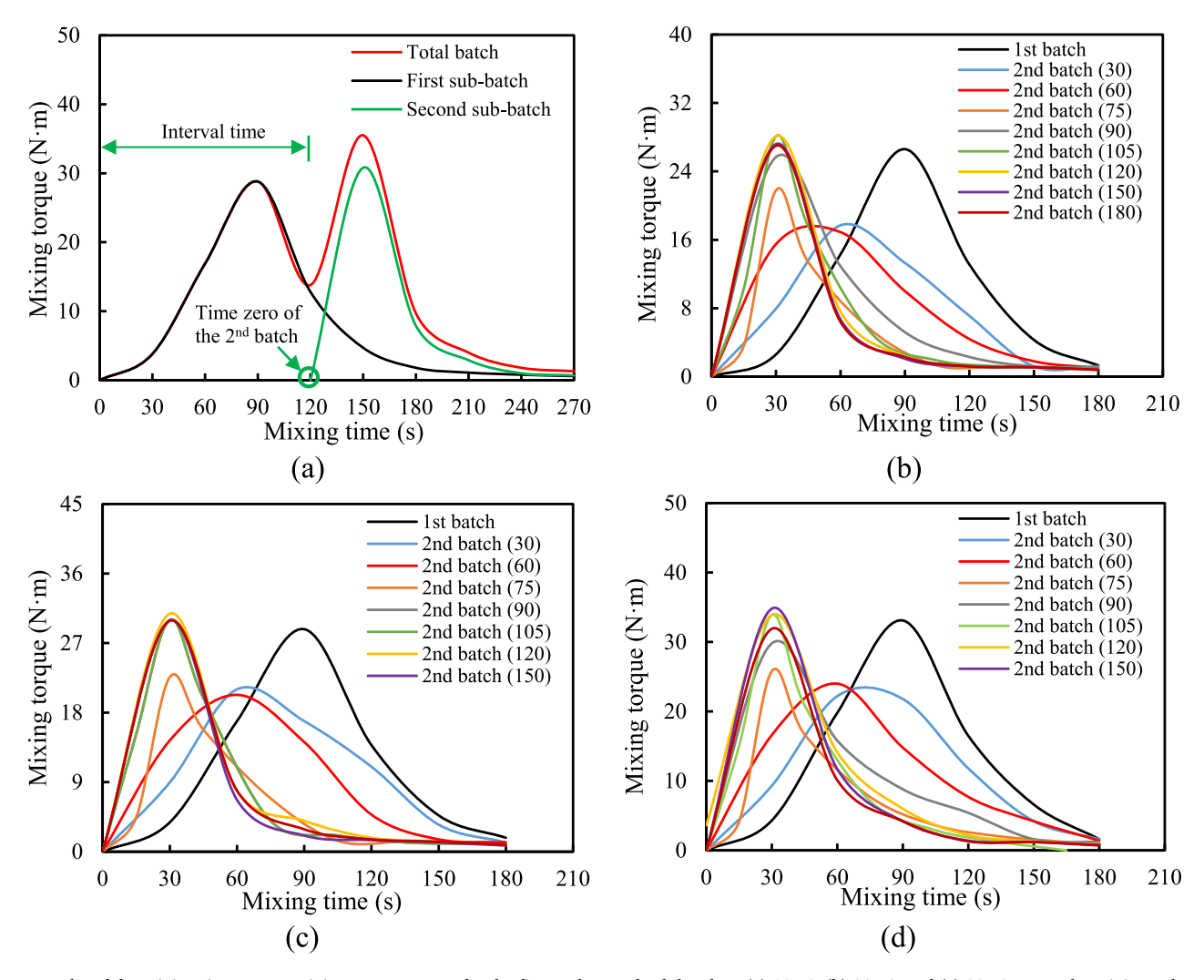


Fig. 7. Results of the mixing time versus mixing torque curves for the first and second sub-batches: (a) 10  $^{\circ}$ C; (b) 20  $^{\circ}$ C; and (c) 30  $^{\circ}$ C. Note: the mixing volume for each sub-batch is 1.5 L.

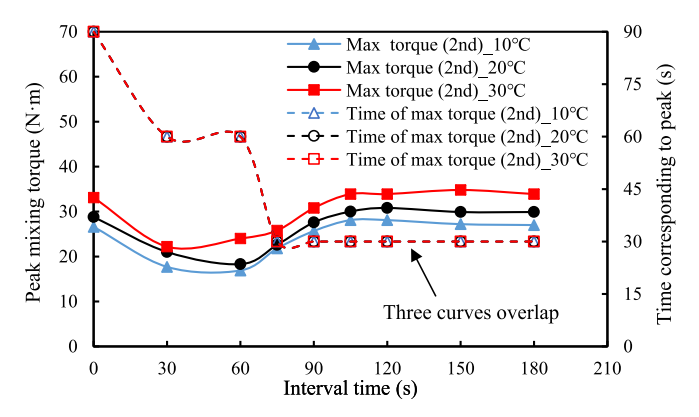


Fig. 8. Trends of the peak mixing torque and time instant corresponding to the second batch.

can be determined by superimposing the evolution curves of mixing torques of all sub-batches, as depicted in Fig. 7(a). The total torque of the two-batching method is determined by the superposition of the two curves of the first and the second sub-batches. In other words, the evolution curve of the second sub-batch can be calculated by subtracting the evolution curve of the first sub-batch from the total curve in the two-batching method. For the sake of comparison of the cases with

different interval times, the curve of the second sub-batch is horizontally shifted to the origin based on the interval time, as shown in Fig. 7(b) to 7 (d). These figures show consistent phenomena: (1) The curve of the second sub-batch was related to the interval time. When the interval time was 90 s or longer, the curves were almost the same. (2) It took shorter time (30 s) for the second sub-batch to reach the peak torque. (3) The magnitude of the peak torque of the second sub-batch was equal to the magnitude of the first sub-batch. These observations indicate interactions between the two sub-batches. In other words, the mixing kinetics of the second sub-batch is dependent on the first sub-batch. In addition, the interval time plays an important role on the mixing kinetics. The underlying mechanism is discussed in Section 3.3.

Fig. 8 manifests the trends of the magnitude of the peak torque and the time corresponding to the peak torque as the interval time was increased from 0 to 180 s. The results from the different temperatures showed consistent phenomena for the magnitude and the time of the peak torque: (1) The magnitude of the peak torque first decreased and then increased, until it stabilized to a value dependent on the temperature. The data for the zero-interval time were obtained from cases M1-1.5-10C, M1-1.5-20C, and M1-1.5-30C. (2) The time corresponding to the peak mixing torque decreased, until it stabilized to 30 s. (3) Both the magnitude of the peak mixing torque and time corresponding to the peak mixing torque were stabilized after the interval time reached 90 s.

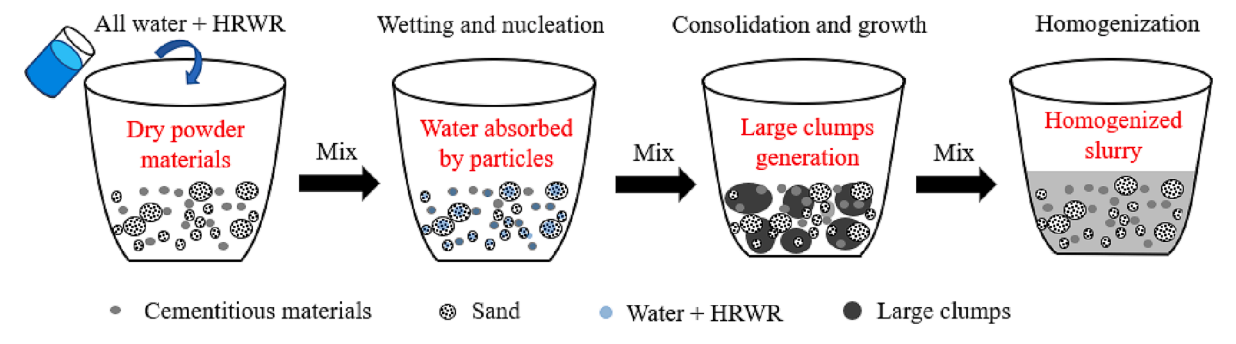


Fig. 9. Illustration of the evolution of the microstructure of UHPC mixtures in the mixing process.

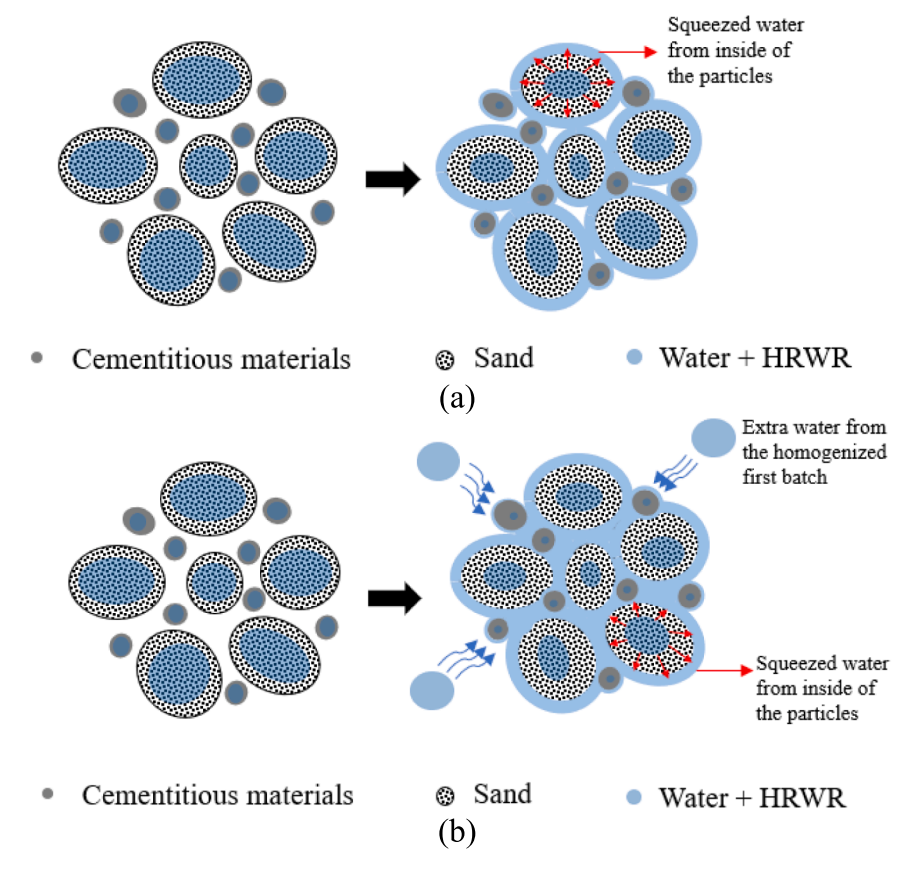


Fig. 10. Schematic diagrams of the microstructure evolution in the consolidation and growth stages: (a) mono-batching method, and (b) multi-batching method.

# 3.3. Evolution of microstructure

Fresh UHPC is a powder-liquid mixture that uses liquid to disperse dry particles through a combination of capillary and viscous forces to form the homogenized slurry [43,44]. This section discusses the evolution of the microstructure for the powder-liquid mixture during the mixing process, in order to reveal the effect of different mixing methods on the evolution of mixing torque. Specifically, the evolution of microstructures explains the changes of particle morphology in the mixing process of UHPC.

The whole mixing process was divided into five stages, which were designated as the wetting, nucleation, consolidation, growth, and homogenization stages [45], as illustrated in Fig. 9. In the wetting and nucleation stages, most of the liquid is absorbed in the granules, and the surfaces remain dry. Thus, limited discrete water-bound granules are formed. The consolidation and growth stages only occur when the surfaces of the granules become wet. The wetting of surfaces results from the presence of extra water in the mixture and/or water squeezed from

the granules. Finally, the powder-liquid mixtures are homogenized.

It is worth noting that the evolution of microstructures for UHPC is different from that for conventional concrete and self-consolidating concrete because the water-to-binder ratio of UHPC is too low to provide extra water to wet the granules. Therefore, the consolidation and growth stages in evolution of microstructures rely on water squeezed from granules, as shown in Fig. 10(a), thus causing higher demand of mixing torque and longer mixing time compared with conventional concrete and self-consolidating concrete.

When the multi-batching method is used, the mixing kinetics of the first sub-batch is the same as the mono-batching method, but the sub-sequent sub-batches are affected by the prior sub-batches. When the interval time is sufficient, the prior sub-batches are homogenized and provide water to wet the granules of the subsequent sub-batches, thus accelerating homogenization of subsequent sub-batches, as depicted in Fig. 10(b). This mixing kinetics explains the observations from Fig. 6 and the reduction mechanism of the mixing torque by the multi-batching method. In a nutshell, the multi-batching method is capable of

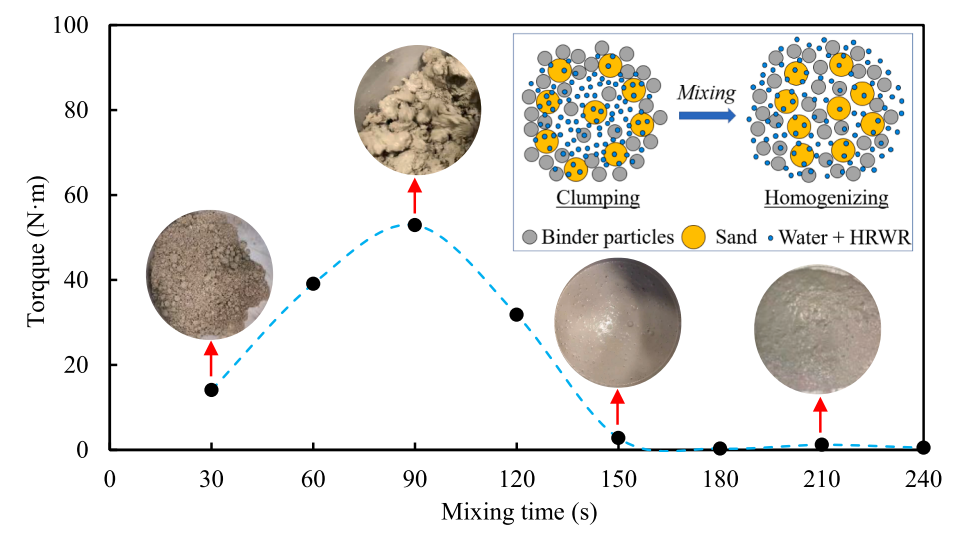
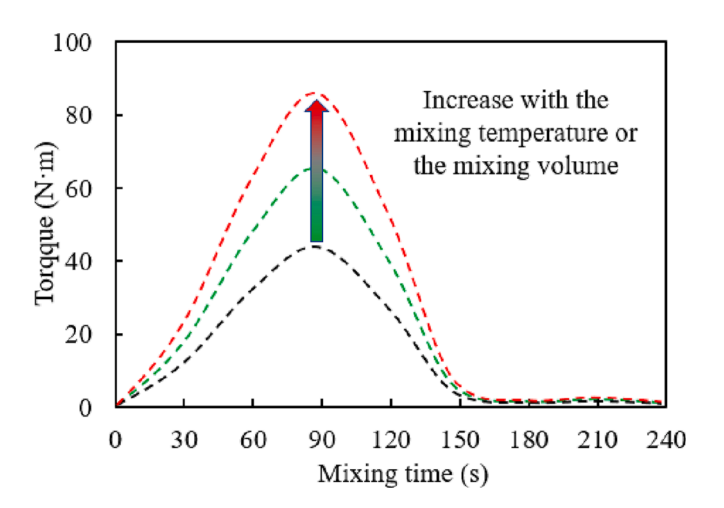


Fig. 11. A representative curve of the evolution of the mixing torque of mono-batching UHPC.



 $\begin{tabular}{ll} {\bf Fig.~12.~Depiction~of~the~effects~of~mixing~temperature~and~mixing~volume~on~the~mixing~torque.} \end{tabular}$ 

reducing the peak mixing torque by staggering the occurrence of the peaks of different sub-batches, which can reduce the malfunction possibility of the mixer in the large-volume UHPC production on job sites.

# 4. Development of mixing kinetics model

# 4.1. Summary of observed phenomena

Fig. 11 shows a representative torque-time curve of mono-batching. The mixing time zero was the time instant when the mixing water and HRWR were added. According to the torque-time curve, the mono-batching process is divided into three phases: (1) Phase I: The torque increases with the mixing time. (2) Phase II: The torque decreases with the mixing time. (3) Phase III: The torque is stabilized. The peak torque occurs at the end of Phase I and the beginning of Phase II.

The mixing torque results in Section 3.1 reveal two important findings: (1) The peak mixing torque is approximately proportional to the mixing temperature, as shown in Fig. 5(a). (2) The peak mixing torque is approximately proportional to the mixing temperature, as shown in Fig. 5(b). Based on the two findings, two hypotheses were proposed for

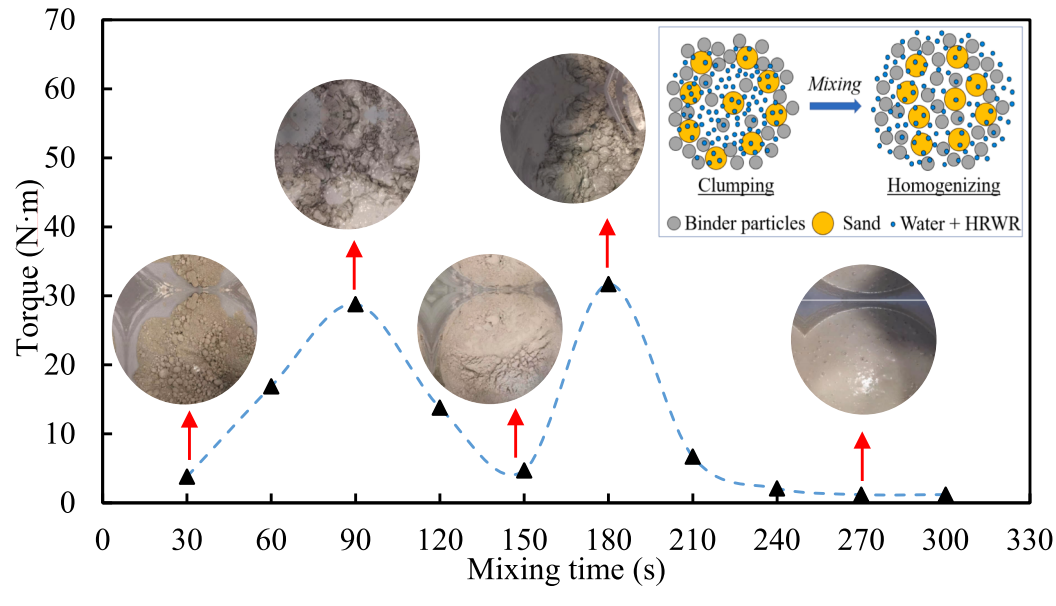
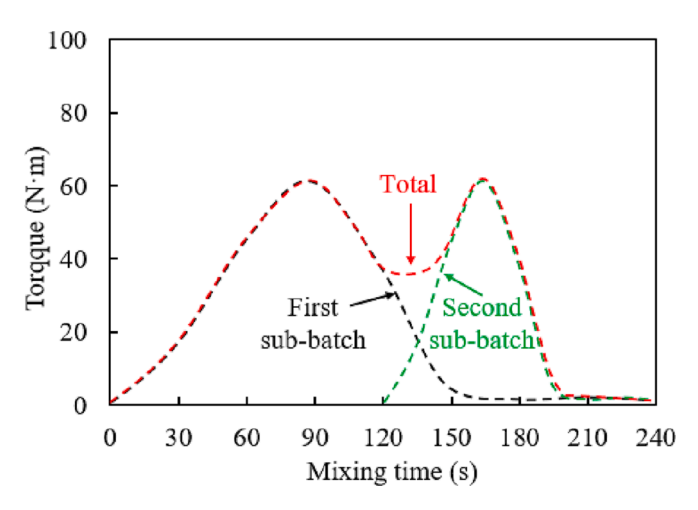


Fig. 13. A representative torque-time curve of the two-batching process of a UHPC mixture M1.



**Fig. 14.** Illustration of the total mixing torque curve by the superposition of the mixing toque curves of the two sub-batches in a representative two-batching case.

Table 4
Calibration of constants of the mixing kinetics model for the mono-batching

Constants	а	b	с	α	β
Optimal value	0.135	65.151	57.785	0.938	0.174

the mixing torque value at an arbitrary time instant, as shown in Fig. 12: (1) The mixing torque is proportional to the mixing temperature. (2) The mixing torque is proportional to the mixing volume.

Fig. 13 shows a representative two-peak curve of the mixing torque for a two-batching case, as elaborated in Section 3.2. According to the curve, the two-batching process is divided into five phases: (1) Phase II: the mixing torque increases with the mixing time. (2) Phase III: the mixing torque decreases with the mixing time. (3) Phase III: the mixing torque increases with the mixing time when the second sub-batch is added. (4) Phase IV: the mixing torque decreases with the mixing time. (5) Phase V: the mixing torque is stabilized. The first peak toque occurs at the end of Phase I and the beginning of Phase II, and the second peak torque occurs at the end of Phase IIII and the beginning of Phase IV. It is clear to see that the mixing torque achieves the second peak with a shorter time than the first peak after the addition of the second sub-batch which is explained in Section 3.3, so the second peak is narrower than the first peak.

The total mixing torque curve of the two-batching method is the superposition of the mixing torque curves of the two sub-batches, as shown in Fig. 14. However, since the mixing process of the second sub-batch is affected by the first sub-batch, the mixing torque curve of the second sub-batch is pinched compared with the mixing torque curve of

**Table 5**Calibration of constants of the mixing kinetics model for the multi-batching cases.

Model constants	а	b	с	α	β
First batch	0.135	65.151	57.785	0.938	0.174
Second batch	0.455	20.788	27.423	0.938	0.174

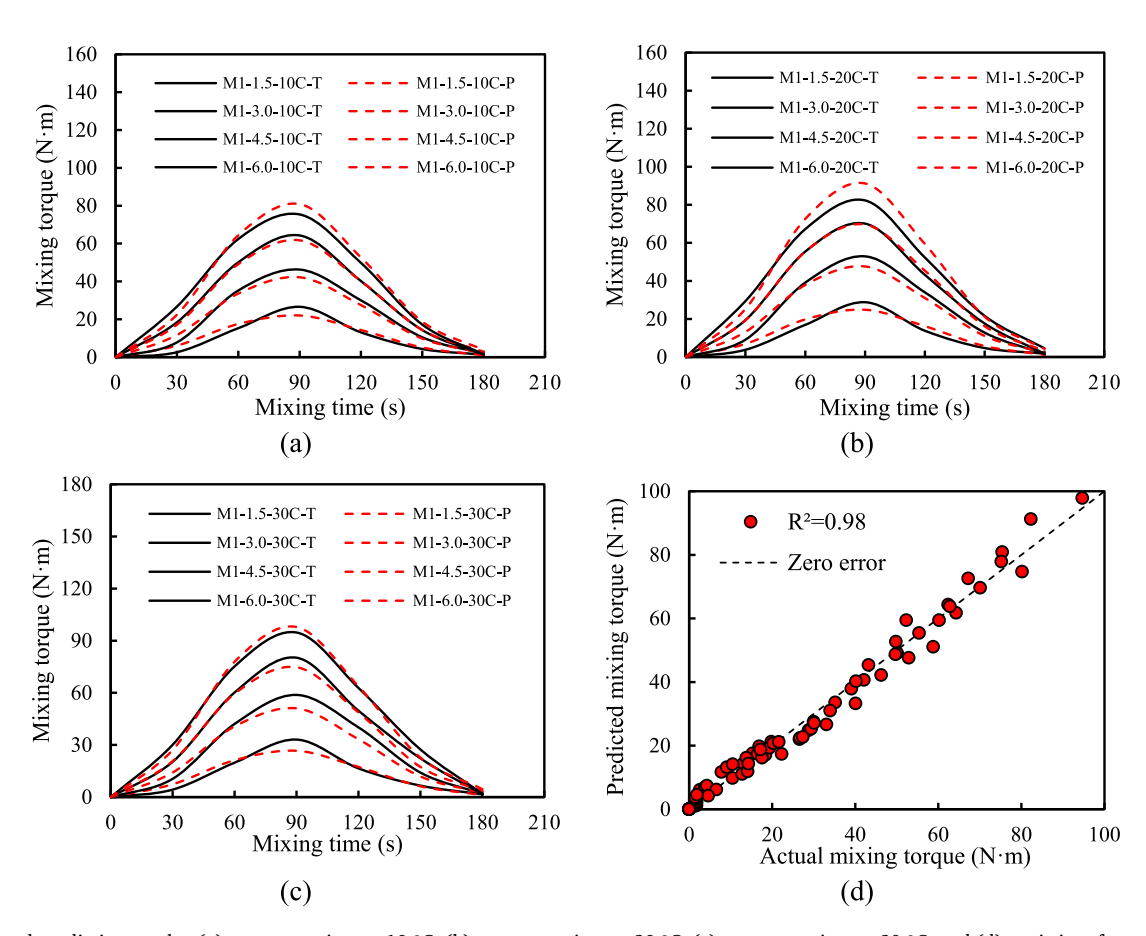


Fig. 15. Test and prediction results: (a) torque vs. time at 10 °C, (b) torque vs. time at 20 °C, (c) torque vs. time at 30 °C, and (d) statistics of comparison. In the designation, T: testing results, P: predicted results.

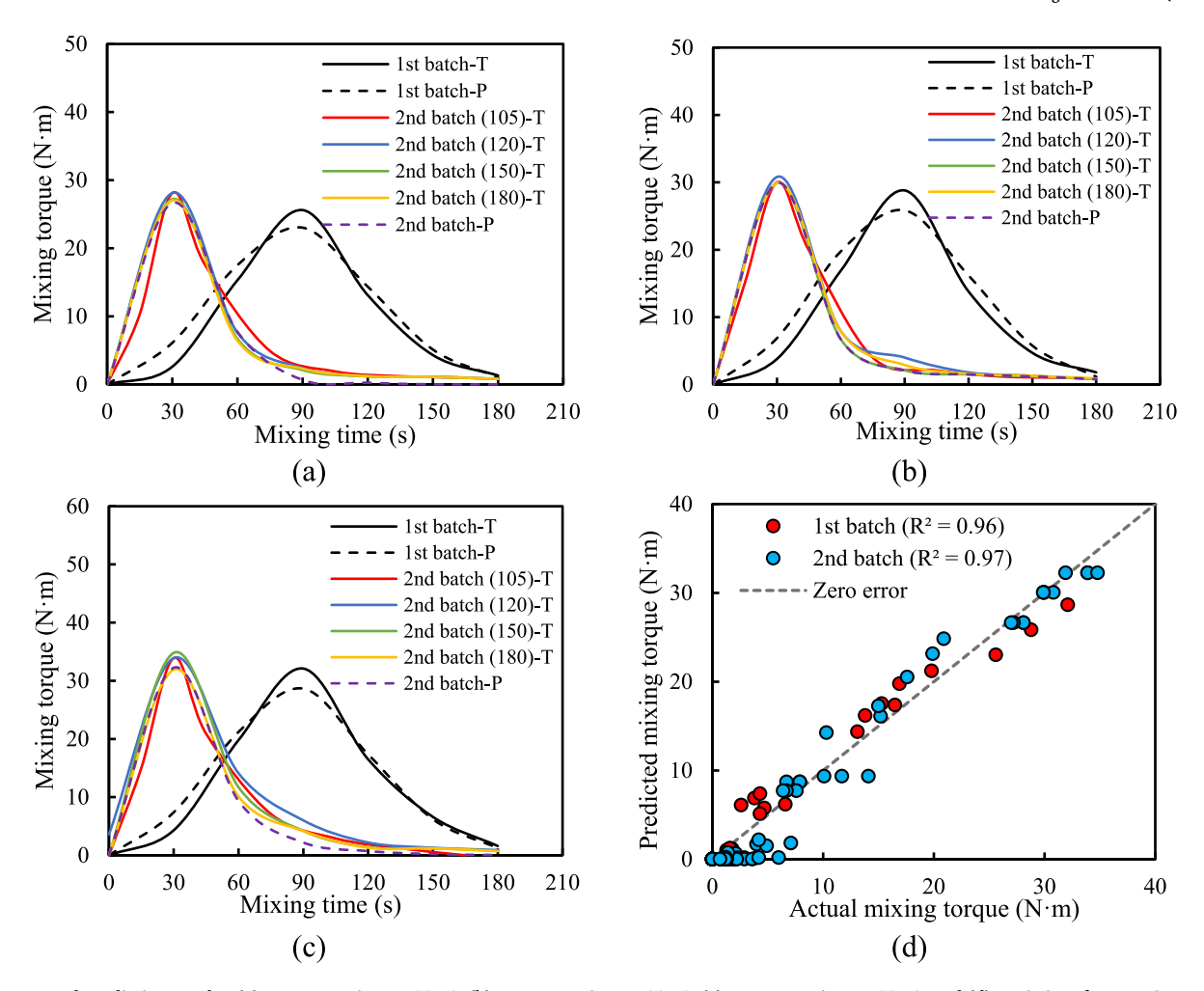


Fig. 16. Test and prediction results: (a) torque vs. time at 10 °C, (b) torque vs. time at 20 °C, (c) torque vs. time at 30 °C, and (d) statistics of comparison. T: testing results, P: predicted results.

the first sub-batch. When the interval time is sufficiently long, the effect of prior batch is stabilized, as depicted in Fig. 7.

# 4.2. Formulation of mixing kinetics model

According to the above observations, the evolution of the mixing torque in the mixing process of UHPC is affected by the mixing volume, mixing temperature, and mixing time. A mixing kinetics model is presented in this section.

#### 4.2.1. Mono-batching cases

According to the experimental results and discussions in Section 3.1, the mixing torque is related to the mixing volume, mixing temperature, and mixing time. And three impact factors are independent. Therefore, a conjecture model is proposed, as expressed in Eq. (1):

$$Q(V,T,t) = A \times f(V) \times g(T) \times h(t)$$
(1)

where Q(V,T,t) represents the mixing torque; A represents the general coefficient; f(V) represents the effect of mixing volume; g(T) represents the effect of mixing temperature; and h(t) represents the effect of mixing time.

Specifically, the mixing torque increased with the mixing temperature and mixing volume. As the mixing time increased, the mixing torque first increased, then decreased, and finally stabilized, similar with the trend of Gaussian distribution curves. Therefore, the conjecture model is rewritten as Eq. (2):

$$Q(V, T, t) = a \times V^{\alpha} \times T^{\beta} \times t \times e^{-\frac{(t-b)^2}{c^2}}$$
(2)

where a, b, c,  $\alpha$ , and  $\beta$  are constants to be calibrated using experimental data; T represents the mixing temperature; V represents the mixing volume; and t represents the mixing time.

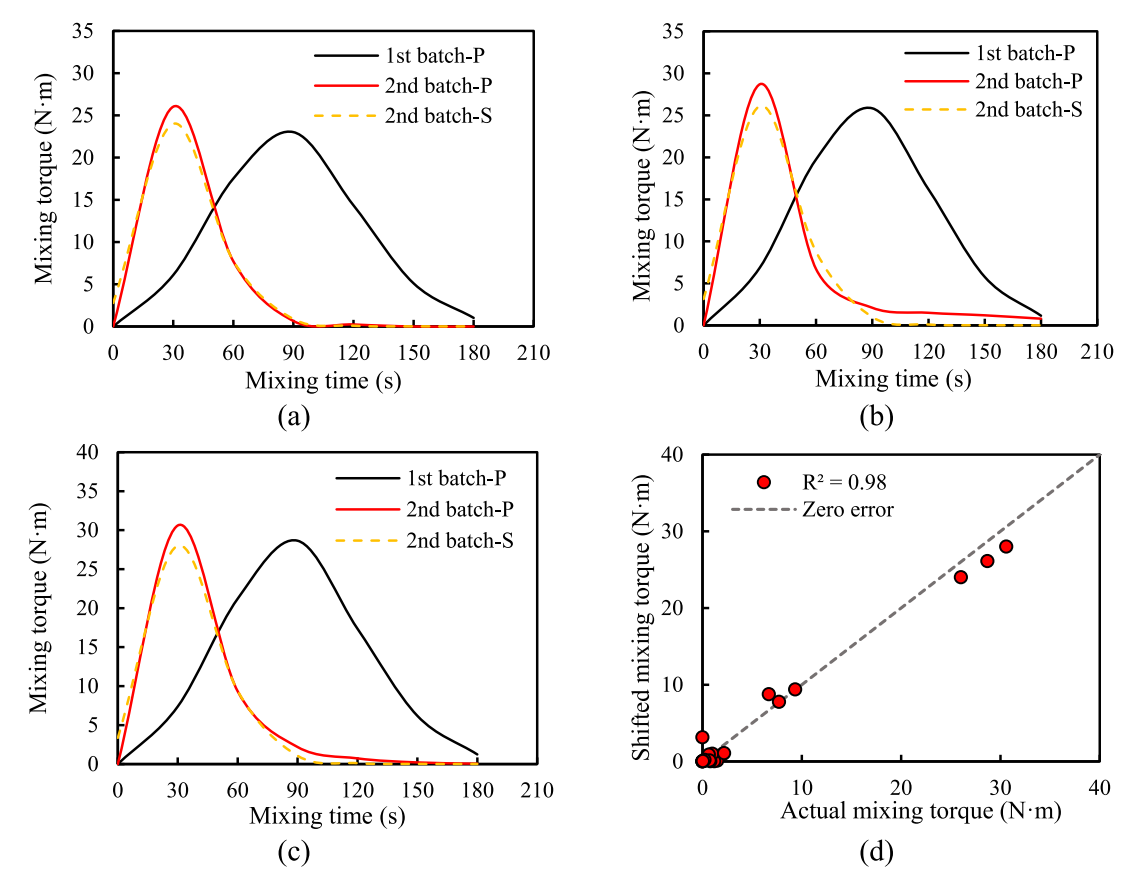
Regression analysis was conducted for the conjecture model using the experimental data from cases C1 to C12. In the regression analysis, the model constants were determined using the lion pride optimization algorithm through an inverse analysis [46,47]. The calibration results of the model constants are listed in Table 4. The mixing torque can be predicted using the model.

Fig. 15(a) to (c) plot the test results shown in black color and prediction results shown in red color for mixture M1 with different mixing temperatures and mixing volume. Fig. 15(d) shows the comparison between the actual mixing torque and the predicted mixing torque. The coefficient of determination  $(R^2)$  value is 0.98, indicating that the presented model was capable of predicting the evolution of the mixing torque.

# 4.2.2. Multi-batching cases

The mixing torque curves of multi-batching cases showed one or multiple peaks, and the prior batches affected the subsequent batches. The total mixing torque was the superposition of mixing torques of all sub-batches, as expressed in Eq. (3).

$$Q_{multi}(t) = Q_1(t) + Q_2(t) + \dots + Q_n(t)$$
(3)



**Fig. 17.** Prediction and transformed results: (a) torque vs. time at 10 °C, (b) torque vs. time at 20 °C, (c) torque vs. time at 30 °C, and (d) statistics of comparison. In the designation, "P" and "S" represent the prediction and transformed results, respectively.

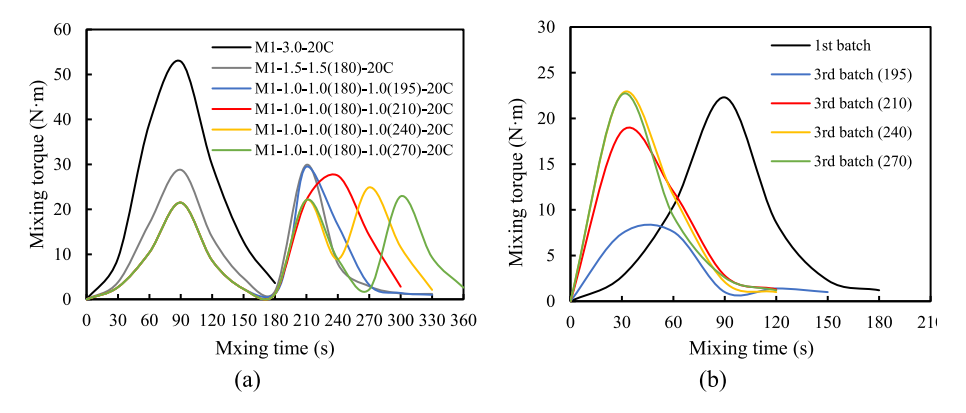


Fig. 18. Results of the mixing torque in the three-batching cases: (a) the total mixing torque; and (b) the mixing torque curves associated with the first and third sub-batches.

 $\begin{tabular}{ll} \textbf{Table 6} \\ \textbf{Calibration of constants of the mixing kinetics model for the multi-batching cases.} \end{tabular}$ 

Model constants	а	b	с	α	β
First batch	0.135	65.151	57.785	0.938	0.174
Second batch	0.455	20.788	27.423	0.938	0.174
Third batch	0.718	0	43.466	0.938	0.174

where  $Q_{multi}$  is the total mixing torque;  $Q_1$  is the mixing torque due to the first sub-batch;  $Q_2$  is the mixing torque due to the second sub-batch;  $Q_n$  is the mixing torque due to the n-th sub-batch.

The two-batching method was used to develop the mixing kinetics

model for multi-batching cases. The data were obtained from cases: C17 to C20, C25 to C28, and C33 to C36. The same formula and inverse analysis method were employed to calibrate the model constants for the second batch while the model constants for the first batch were sustained. The test results showed that the mixing torque associated with the second sub-batch was dependent on the interval time between the first and second sub-batches, but when the interval time was longer than 90 s, the mixing torque associated with the second sub-batch was independent on the interval time. Here, to exemplify the method, only the constants of the stabilized curves are presented in Table 5.

Fig. 16(a) to (c) plot the test and prediction results for the first and second sub-batches at 10  $^{\circ}$ C, 20  $^{\circ}$ C, and 30  $^{\circ}$ C, respectively. Fig. 16(d) shows the comparison between the actual mixing torque and the

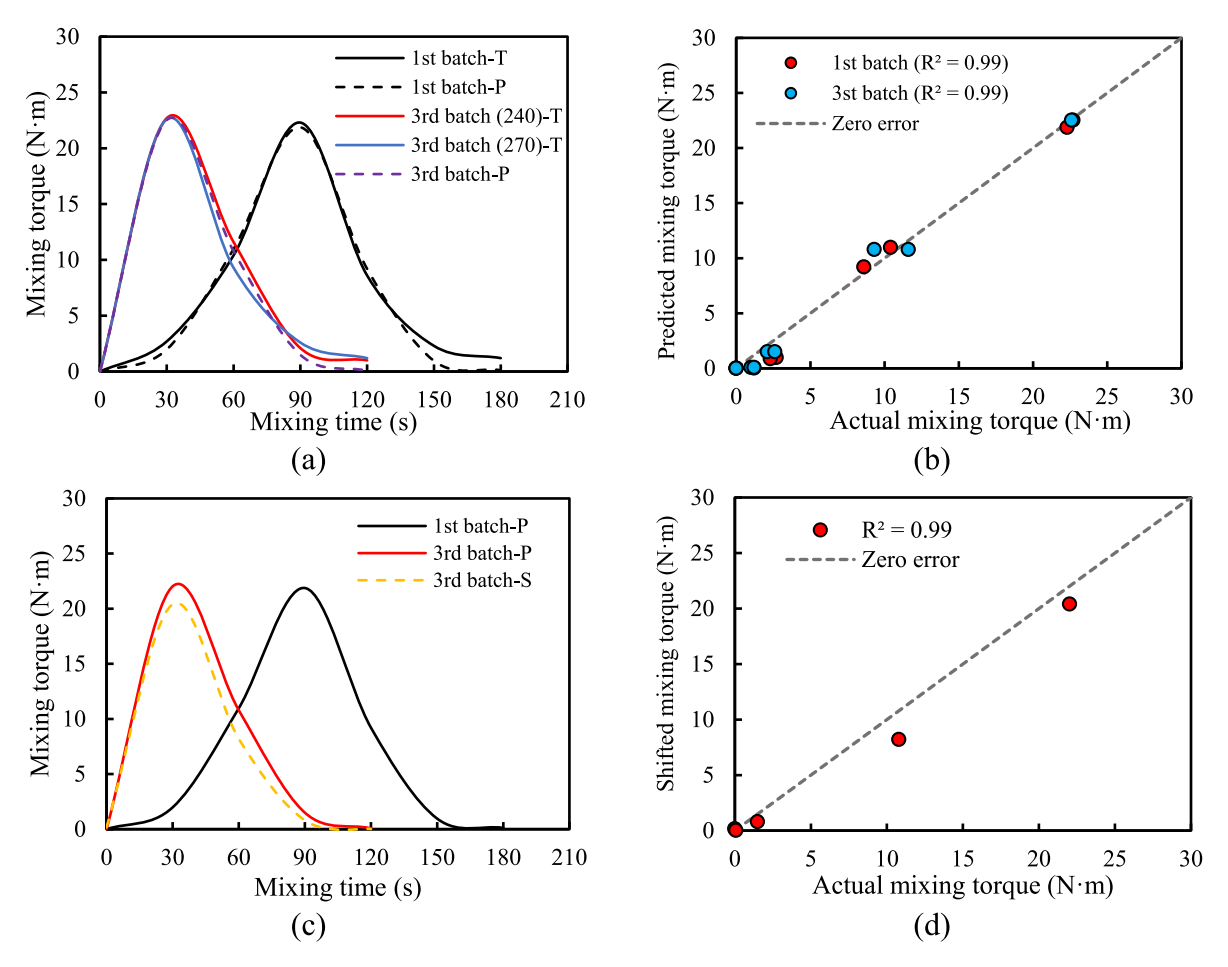


Fig. 19. Comparison of test and prediction results: (a) test and prediction of mixing torque at 20 °C, (b) comparison of test and prediction results, (c) prediction and transformation of mixing torque at 20 °C, and (d) comparison of prediction and transformation results.

**Table 7**Fresh properties of validation UHPC mixtures.

Mixture design	Mini-slump spread (mm)	Flow time (s)
M1	$275\pm10$	$35 \pm 2.2$
M2	$255\pm10$	$42\pm2.7$
M3	$238\pm10$	$51\pm1.4$
M4	$220\pm10$	$59\pm1.8$

predicted mixing torque based on the fitting curves. The  $R^2$  values are higher than 0.96, indicating that the presented model was capable of predicting the mixing torque.

# 4.2.3. Correlation between sub-batches

Although test data can be used to calibrate the model constants of the mixing torque of the subsequent sub-batches when the multi-batching method is used, it is time consuming to generate the test data from many multi-batching cases. To facilitate applications of the proposed method, further research was conducted to explore the relationship between the evolution curves of the mixing torque of the first and subsequent sub-batches.

Based on the discussions on the mixing kinetics in Section 3.3, it is hypothesized that the mixing torque of the subsequent sub-batches can be obtained by transforming the mixing torque curve of the first sub-batch. According to this hypothesis, the concept of transformed mixing time is proposed to relate the evolution curves of subsequent sub-batches to the evolution curve of the first sub-batch. The mixing torque of the subsequent sub-batches is expressed as:

$$Q_s(t) = a \times V^{\alpha} \times T^{\beta} \times t_s \times e^{-\frac{(s-b)^2}{c^2}}$$
(4)

where t is the real mixing time;  $t_s$  is the transformed mixing time, and  $Q_s()$  represents the mixing torque formulated using the transformed mixing time.

With the test data from a total of 12 cases, which are cases C17 to C20, C25 to C28, and C33 to C36, the relationship between the real mixing time and the transformed mixing time was obtained from a regression analysis, as shown in Eq. (5).

$$t_s = -0.0068 \times t^2 + 2.4348 \times t + 18.2301 \tag{5}$$

Fig. 17(a) to (c) plot the prediction curves and transformed curves for the first batch and second sub-batches at 10 °C, 20 °C, and 30 °C, respectively. Fig. 17(d) shows the comparison between the actual mixing torque and the shifted mixing torque. The  $R^2$  value is 0.98, indicating that the transformation curve was capable of predicting the mixing torque.

# 4.3. Model validation

# 4.3.1. Three-batching cases

Fig. 18(a) plots the mixing torque curves of cases C5, C28, and C46 to C49 for mixture M1. Three peaks of mixing torque were produced when the time interval was 60 s or longer. The peak mixing torque was further reduced to 22.9 N·m. Fig. 18(b) plots the mixing torque curves of the

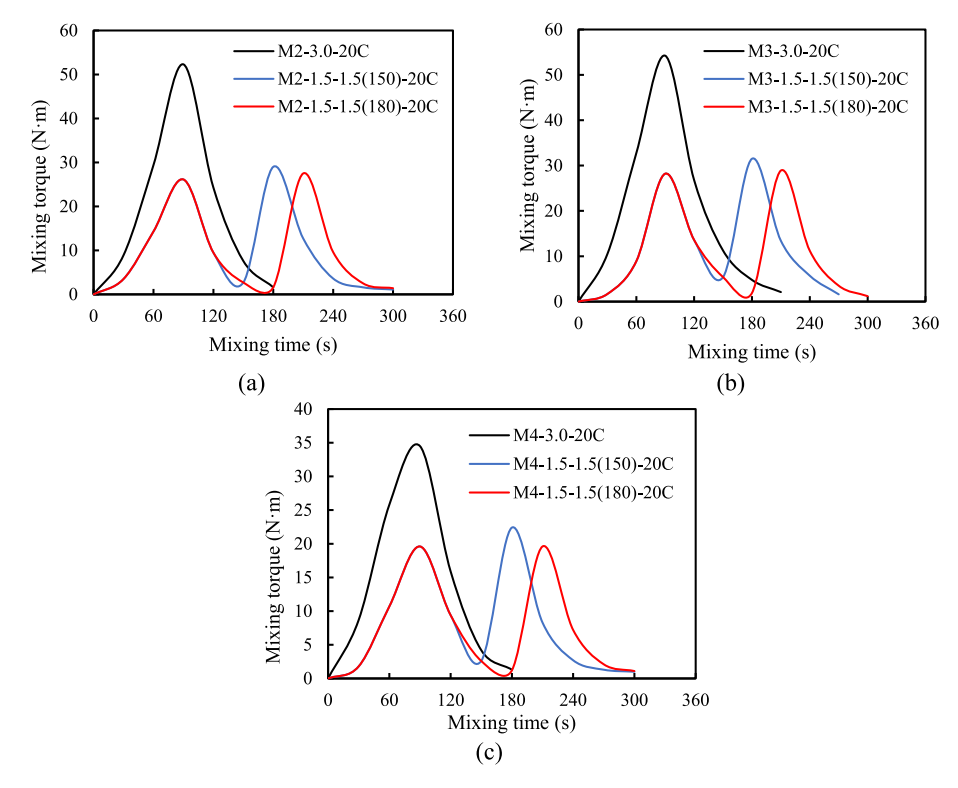


Fig. 20. Test results of the mixing torque versus mixing time for: (a) M2 (b) M3, and (c) M4.

**Table 8**Calibration of constants of the mixing kinetics model for different UHPC mixtures.

Model constants		а	b	с	α	β
M2	First batch	0.128	77.843	36.942	0.938	0.174
	Second batch	0.610	0	41.507	0.938	0.174
M3	First batch	0.125	87.353	34.305	0.938	0.174
	Second batch	0.639	0	42.877	0.938	0.174
M4	First batch	0.093	79.267	40.410	0.938	0.174
	Second batch	0.468	0	41.093	0.938	0.174

first and third sub-batches. When the time interval was 60 s or longer, the mixing torque curves of the subsequent sub-batches were stabilized. The same regression analysis method was performed to calibrate the model constants for the three-batching cases, as listed in Table 6.

Fig. 19(a) compares the test and prediction results for the first and third sub-batches at 20 °C. Fig. 19(b) shows the comparison between the actual mixing torque and the predicted mixing torque. The  $\mbox{\it R}^2$  values are 0.99, indicating that the presented model was capable of predicting the mixing torque. Fig. 19(c) compares the prediction and transformed results of the third sub-batch at 20 °C. Fig. 19(d) shows the comparison between the prediction and transformed results of the mixing torque. The  $\mbox{\it R}^2$  value is 0.99, indicating that the transform relationship was capable of predicting the mixing torque.

#### 4.3.2. Different UHPC mixtures

The presented mixing kinetics model was validated using different UHPC mixtures listed in Table 2. Table 7 lists the mini-slump spread and flow time of mixtures M1 to M4. The test data of mixing torque from cases C37 to C45 are used to test the performance of the mixing kinetics model.

Fig. 20 plots the mixing torque curves for mixtures M2, M3, and M4, respectively. The results were consistent with the results from mixture M1. The two-batching method led to two peaks of mixing torque. The second peak decreased with the interval time and became stabilized. The

peak mixing torque of the mono-batching method was higher than that of the multi-batching method. The results reveal that the fresh properties of UHPC mixtures affected the absolute value of the mixing torque but did not change the trend.

Using the same regression analysis method, the model constants of mixtures M2 to M4 were calibrated. Table 8 lists the constants of the mixing kinetics model for the three UHPC mixtures. The calibration results show that constants  $\alpha$  and  $\beta$  are the same for the different UHPC mixtures.

Fig. 21(a) to 21(c) plot the test and prediction results for the first and second sub-batches for mixtures M2, M3, and M4, respectively. Fig. 21 (d) shows the comparison between the actual and the prediction results of the mixing torque. The  $\rm R^2$  value is 0.97, indicating that the presented mixing kinetics model was capable of reasonably predicting the evolution of the mixing torque for different UHPC mixtures.

Results indicated that, even though the raw materials (or viscosity) of UHPC mixtures and the number of sub-batches were changed, the mixing kinetics model, proposed in Eq. (2) and Eq. (3), still can well predict the mixing torque evolution during the UHPC production process by using different mixing methods. Therefore, the developed mixing kinetics model is a general model, which can be used for different mixing designs and different mixing methods. The only point is that the specific coefficients are different for different mixture designs and mixing methods, which are obtained from the regression analysis.

# 5. Key properties and characteristics of UHPC mixtures

This section evaluates the effect of the multi-batching method on the workability such as the mini slump spread and flow time, autogenous shrinkage, compressive strength, and hydration kinetics of UHPC mixtures. Specifically, for the 2-batching method, the time interval between 1st sub-batch and 2nd sub-batch is 180 s. In addition, for the 3-batching method, the time interval between 1st sub-batch and 2nd sub-batch is 180 s as well as the time interval between 1st sub-batch and 3rd sub-batch is 270 s.

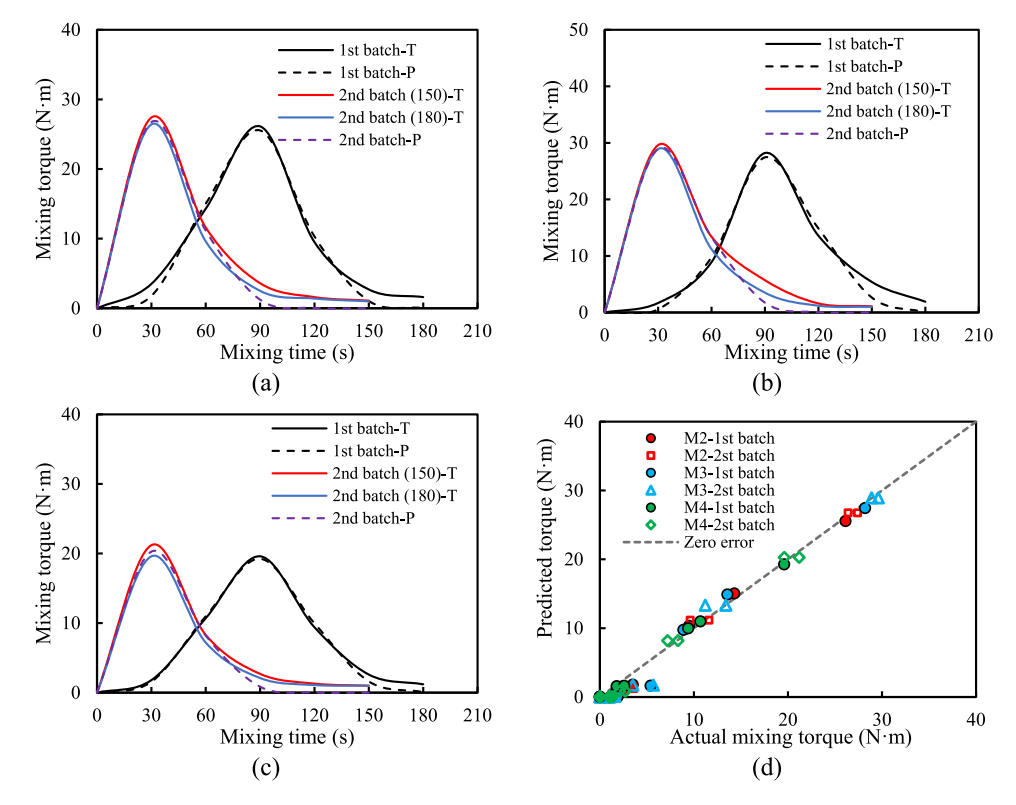


Fig. 21. Test and prediction results: (a) M2, (b) M3, (c) M4, and (d) statistics of comparison.

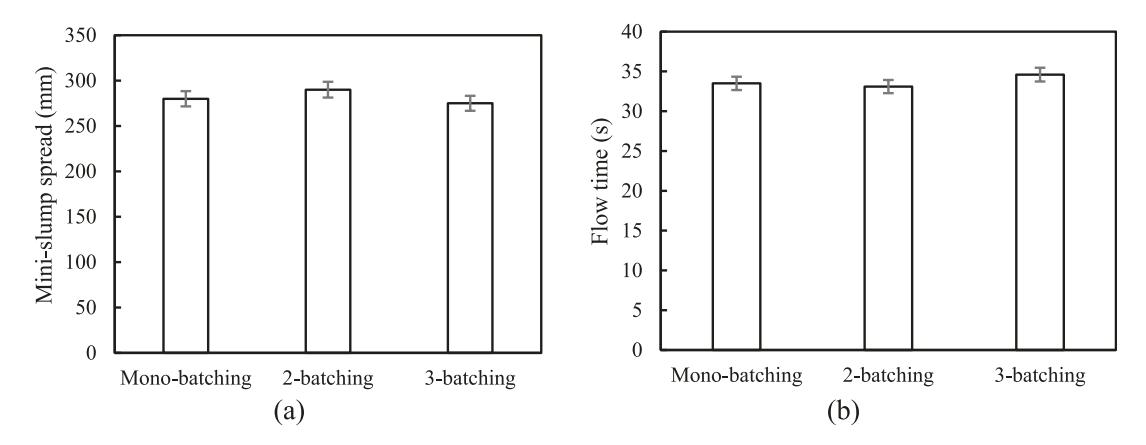


Fig. 22. Test results of the fresh properties of UHPC mixture M1 mixed using different methods: (a) mini slump spread; and (b) flow time.

# 5.1. Fresh and hardened properties

Fresh properties were evaluated by testing the mini-slump spread in accordance with ASTM C230/C230M [48] and mini V-funnel flow time in accordance with EFNARC recommendations [49]. The hardened properties were evaluated by testing the compressive strength using 50-mm cubes, in accordance with ASTM C109 [50]. Immediately after casting, the specimens were covered by wet burlap and plastic sheet. The specimens were demolded after 1 d, and then cured in lime-saturated water at room temperature (23  $\pm$  2 °C) until testing. The loading rate was kept constant at 1.8 kN/min. The compressive tests were conducted at 1, 3, 7, 14, and 28 d. Fig. 22 shows the mini-slump spread and flow time of mixture M1 from cases C5, C28, and C49, which represent monobatching, two-batching, and three-batching, respectively. The mixing temperature and mixing volume were kept at 20 °C and 3 L, respectively. The test results showed that the mini-slump spread was in the range of 280  $\pm$  10 mm, and the flow time was in the range of 33.7  $\pm$  1.7 s. The

multi-batching methods did not affect the fresh properties of UHPC.

In addition, considering that the friction between particles with mixing paddle might affect the temperature of UHPC mixtures and the multi-batching method involved longer mixing time than the monobatching method. The temperature of the UHPC mixtures in the mixing process was measured. Fig. 23 plots the temperature of mixture M1. For mono-batching method, the temperature slightly increased with the mixing time. After the mixture was mixed for 180 s, the temperature increase was in the range of 2  $^{\circ}$ C to 4  $^{\circ}$ C. For the two-batching method, the temperature of mixture M1 first increased with the mixing time, slightly decreased when the second sub-batch was added, and then gradually increased again. After the mixture was mixed for 300 s, the temperature change was also in the range of 2  $^{\circ}$ C to 4  $^{\circ}$ C. In summary, the temperature change was relatively small and consistent for the different mixing methods.

Fig. 24 shows the effects of the compressive strength of mixture M1 from cases C5, C28, and C49. The test results of the compressive strength

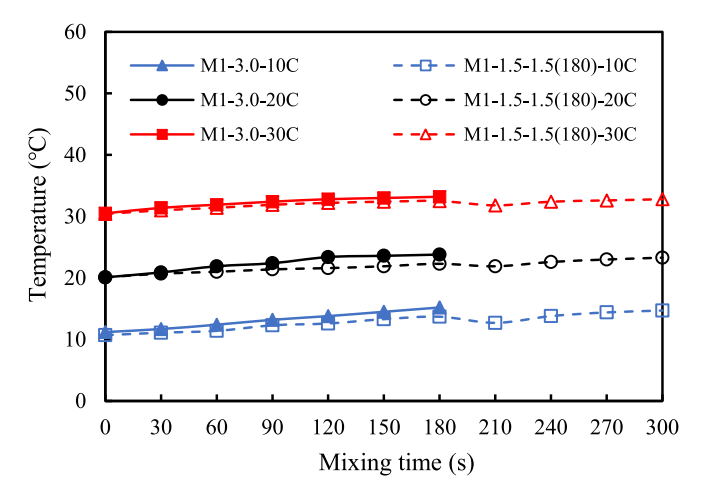


Fig. 23. Measurement results of the temperature of mixture M1 at different mixing temperatures.

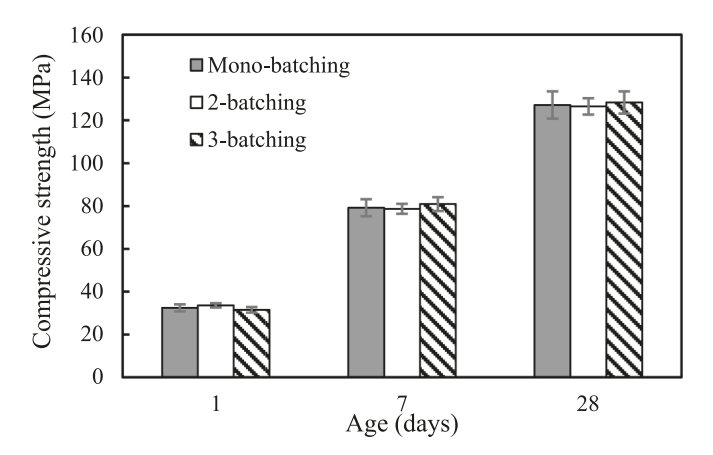


Fig. 24. Test results of the compressive strength of mixture M1 mixed using different methods.

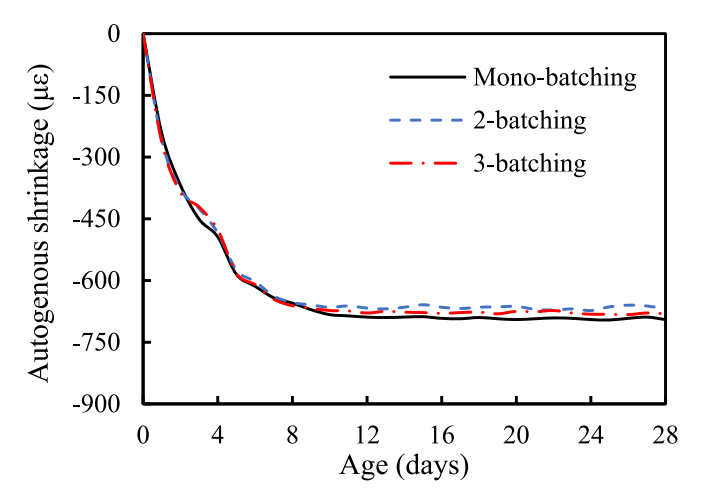


Fig. 25. Test results of the autogenous shrinkage of mixture M1 mixed using different methods.

indicate that the proposed multi-batching method did not affect the compressive strength.

# 5.2. Autogenous shrinkage

The autogenous shrinkage was evaluated according to ASTM C1698 [51]. The final setting time instant was regarded as time zero, in accordance with ASTM C403 [52]. The specimens measure 25 mm  $\times$  25 mm  $\times$  280 mm and were sealed with a water-proof alumina tape to prevent moisture loss. Fig. 25 shows the autogenous shrinkage of mixture M1 from cases C5, C28, and C49. The test results indicate that the proposed multi-batching method did not affect the autogenous shrinkage.

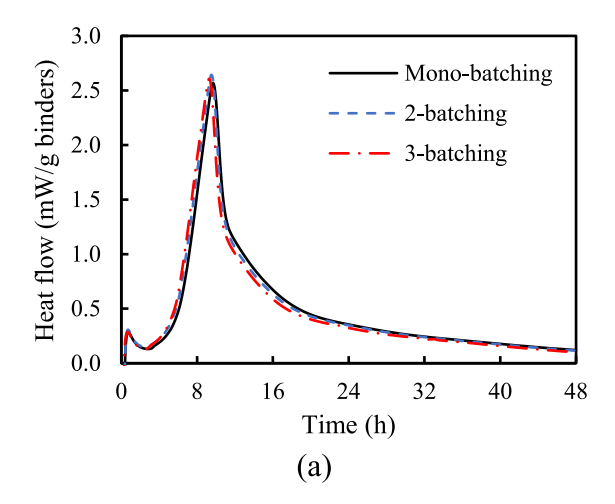
# 5.3. Hydration kinetics

The hydration kinetics of each mixture was evaluated using an isothermal calorimeter (model: Calmetrix I-Cal 4000 HPC). Temperature of samples was maintained at  $25\,^{\circ}\text{C}$ . About  $60\,\text{g}$  of the fresh mixture was sealed in a plastic vial and placed in the calorimeter. The heat of hydration was normalized by binder mass and continuously measured until 48 h after completion of mixing. Fig. 26 shows the hydration kinetics of mixture M1 from cases C5, C28, and C49. The test results indicate that the proposed multi-batching method did not affect the hydration kinetics.

# 6. Conclusions

This study investigates the effect of mixing volumes, mixing temperatures, and mixing method on mixing kinetics of UHPC for the first time. Besides, the multi-batching method is validated to facilitate the large-scale UHPC production. More importantly, a mathematical mixing kinetics model was developed to quantify the mixing torque evolution of UHPC mixtures. Different mixtures and mixing methods were designed to validate the reliability and repeatability. The following conclusions are drawn:

- (1) The mixing kinetics of UHPC is different with conventional concrete. Due to the low w/b and high binder contents, the consolidation and growth stages for UHPC can only depend on the squeezed water from particles, which significantly increases the peak mixing torque and prolongs the mixing time during the mixing process.
- (2) The mixing kinetics of UHPC is closely associated with the mixing temperature, mixing volume, mixing method, and mixing time. Results indicates that the peak mixing torque linearly increases with the mixing temperature and mixing volume. More importantly, the peak mixing torque is more sensitive to the mixing volume.
- (3) The presented multi-batching method can significantly reduce the peak mixing torque. Compared to the mono-batching method (case C5), the peak mixing torque is reduced by 44% for the twobatching method (case C28) and 59% for the three-batching method (case C49). The mechanism is that the homogenized prior sub-batches helps wet the surface of solid particles in subsequent sub-batches, thus accelerating the mixing process of subsequent sub-batches.
- (4) The adoption of multi-batching method shows negligible effects on fresh and hardened properties of UHPC mixtures, including mini slump spread, flow time, compressive strength, and autogenous shrinkage, as well as the hydration kinetics of UHPC mixtures. The multi-batching method is promising to facilitate the large-scale UHPC production.
- (5) A mathematical mixing kinetics model is proposed for the first time to quantify the mixing torque evolution for UHPC mixtures by considering mixing temperature, mixing volume, mixing



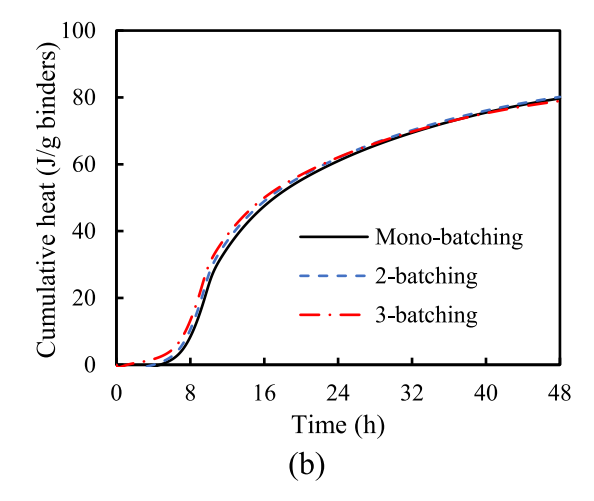


Fig. 26. Test results of the hydration heat of mixture M1: (a) heat flow; and (b) cumulative heat.

**Table A1**The detail information of the mixer in this study.

Brand	Hobart	
Model Horsepower	HL-200 0.5 hp	
Output Capacity	0.5 np 11.5 L	
Attachment	Flat beater	
Mixing Speed (adopted in this study)	Agitator (RPM)	Attachment (RPM)
	107	61

method, and mixing time (R $^2 \geq 95\%$ ). The reliability, repeatability, and generalization of the presented mixing kinetics model are verified through the validation tests with different UHPC mixtures and mixing methods.

(6) The limitation of the presented model is that more experimental data from other labs about the mixing torque evolution for UHPC mixtures will be needed to further optimize the mixing kinetics model.

# CRediT authorship contribution statement

Jiang Du: Data curation, Formal analysis, Investigation, Visualization, Writing – original draft. Soroush Mahjoubi: Data curation, Investigation, Writing – review & editing. Yi Bao: Data curation, Validation, Writing – review & editing. Nemkumar Banthia: Writing – review & editing. Weina Meng: Conceptualization, Project administration, Resources, Supervision, Funding acquisition, Writing – review & editing.

# **Declaration of Competing Interest**

The authors declare that they have no known competing financial interests or personal relationships that could have appeared to influence the work reported in this paper.

# Data availability

Data will be made available on request.

# Acknowledgement

This research is supported by National Science Foundation, United States [grant number CMMI-2046407] and New Jersey Department of Transportation: Task Order 388 – Bridge Resource Program (2021-2022), contract ID number: 21-50862. The authors also would like to

thank Mr. Bill Kulish (the president of Steelike lnc) for the donation of steel fibers.

# **Appendix**

# References

- [1] K. Wille, A.E. Naaman, G.J. Parra-Montesinos, Ultra-high performance concrete with compressive strength exceeding 150 MPa (22 ksi): a simpler way, ACI Mater. J. 108 (1) (2011) 46–54.
- [2] Du, J., Meng, W., Khayat, K. H., Bao, Y., Guo, P., Lyu, Z., Abu-obeidah, A., Nassif, H., and Wang, H., 2021. New development of ultra-high-performance concrete (UHPC). Composites Part B: Engineering, p. 109220.
- [3] Perry, V. 2018. What really is ultra-high performance concrete Towards a global definition. in Proceedings of the 2nd International Conference on UHPC Materials and Structures. RILEM Publications.
- [4] H. Huang, X. Gao, L.e. Teng, Fiber alignment and its effect on mechanical properties of UHPC: an overview, Constr. Build. Mater. 296 (2021) 123741.
- [5] C. Shi, Z. Wu, J. Xiao, D. Wang, Z. Huang, Z. Fang, A review on ultra high performance concrete: Part I. Raw materials and mixture design, Constr. Build. Mater. 101 (2015) 741–751.
- [6] D. Wang, C. Shi, Z. Wu, J. Xiao, Z. Huang, Z. Fang, A review on ultra high performance concrete: Part II. Hydration, microstructure and properties, Constr. Build. Mater. 96 (2015) 368–377.
- [7] J. Li, Z. Wu, C. Shi, Q. Yuan, Z. Zhang, Durability of ultra-high performance concrete – a review. Constr. Build. Mater. 255 (2020) 119296.
- [8] R. Yu, P. Spiesz, H. Brouwers, Mix design and properties assessment of ultra-high performance fibre reinforced concrete (UHPFRC), Cem. Concr. Res. 56 (2014) 29–39
- [9] H. Huang, L.e. Teng, K.H. Khayat, X. Gao, F. Wang, Z. Liu, For the improvement of mechanical and microstructural properties of UHPC with fiber alignment using carbon nanotube and graphite nanoplatelet, Cem. Concr. Compos. 129 (2022), 104462.
- [10] L. Li, B. Wang, M.H. Hubler, Carbon nanofibers (CNFs) dispersed in ultra-high performance concrete (UHPC): Mechanical property, workability and permeability investigation, Cem. Concr. Compos. 131 (2022), 104592.
- [11] H. Huang, R. Wang, X. Gao, Improvement effect of fiber alignment on resistance to elevated temperature of ultra-high performance concrete, Compos. B Eng. 177 (2019), 107454.
- [12] T. Alahmari, C. Kennedy, A. Cuaron, B. Weldon, D. Jauregui, Field testing of a prestressed concrete bridge with high performance and locally developed ultrahigh performance girders, Frontiers in Built Environment 5 (2019) 114.
- [13] Aaleti, S., Sritharan, S., and Abu-Hawash, A. Innovative UHPC-normal concrete composite bridge deck. in Proceedings of the RILEM-fib-AFGC International Symposium on Ultra-High Performance Reinforced Concrete, Eds: F. Toutlemonde, J. Resplendino, Rilem Publications SARL, Bagneux, France. 2013.
- [14] T.V. Voort, M.T. Suleiman, S. Sritharan, Design and performance verification of ultra-high performance concrete piles for deep foundations, Iowa State University. Center for Transportation Research and Education, 2008.
- [15] J. Qi, Y.i. Bao, J. Wang, L. Li, W. Li, Flexural behavior of an innovative dovetail UHPC joint in composite bridges under negative bending moment, Eng. Struct. 200 (2019), 109716.
- [16] Graybeal, B., Field-cast UHPC connections for modular bridge deck elements. 2010.

- [17] B.A. Graybeal, Ultra-high performance concrete composite connections for precast concrete bridge decks., United States, Federal Highway Administration, Office of Infrastructure Research and Development, 2012.
- [18] S. Verger-Leboeuf, J.-P. Charron, B. Massicotte, Design and behavior of UHPFRC field-cast transverse connections between precast bridge deck elements, J. Bridg. Eng. 22 (7) (2017), 04017031.
- [19] J. Xie, Q. Fu, J.-B. Yan, Compressive behaviour of stub concrete column strengthened with ultra-high performance concrete jacket, Constr. Build. Mater. 204 (2019) 643–658.
- [20] Z.B. Haber, J.F. Munoz, B.A. Graybeal, Field testing of an ultra-high performance concrete overlay, Federal Highway Administration. Office of Infrastructure Research & DevelopmentFederal Highway Administration, 2017.
- [21] Khayat, K. H. and Valipour, M., Design of ultra high performance concrete as an overlay in pavements and bridge decks. 2014, Missouri University of Science and Technology. Center for Transportation Infrastructure and Safety.
- [22] Z.B. Haber, J.F. Munoz, I. De la Varga, B.A. Graybeal, Bond characterization of UHPC overlays for concrete bridge decks: Laboratory and field testing, Constr. Build. Mater. 190 (2018) 1056–1068.
- [23] Wibowo, H. and Sritharan, S., Use of Ultra-High-Performance Concrete for Bridge Deck Overlays. 2018, United States. Federal Highway Administration.
- [24] J. Yang, R. Chen, Z. Zhang, Y. Zou, J. Zhou, J. Xia, Experimental study on the ultimate bearing capacity of damaged RC arches strengthened with ultra-high performance concrete, Eng. Struct. 279 (2023), 115611.
- [25] Y. Zou, J. Jiang, J. Yang, Z. Zhang, J. Guo, Enhancing the toughness of bonding interface in steel-UHPC composite structure through fiber bridging, Cem. Concr. Compos. 137 (2023), 104947.
- [26] Y. Zou, K. Zheng, Z. Zhou, Z. Zhang, J. Guo, J. Jiang, Experimental study on flexural behavior of hollow steel-UHPC composite bridge deck, Eng. Struct. 274 (2023), 115087.
- [27] Y. Bae, S. Pyo, Ultra-high performance concrete (UHPC) sleeper: Structural design and performance, Eng. Struct. 210 (2020), 110374.
- [28] Y. Bae, S. Pyo, Effect of steel fiber content on structural and electrical properties of ultra-high performance concrete (UHPC) sleepers, Eng. Struct. 222 (2020), 111131
- [29] J. Du, Z. Liu, C. Christodoulatos, M. Conway, Y.i. Bao, W. Meng, Utilization of off-specification fly ash in preparing ultra-high-performance concrete (UHPC): Mixture design, characterization, and life-cycle assessment, Resour. Conserv. Recycl. 180 (2022), 106136.
- [30] Y. Li, J. Yin, Q. Yuan, T. Huang, J. He, J. Li, Fresh and hardened properties of cement paste and mortar incorporating calcined cutter soil mixing residue, Constr. Build. Mater. 357 (2022), 129376.
- [31] Y. Li, S. Eyley, W. Thielemans, Q. Yuan, J. Li, Valorization of deep soil mixing residue in cement-based materials. Resour. Conserv. Recycl. 187 (2022), 106597.
- [32] W. Meng, M. Valipour, K.H. Khayat, Optimization and performance of cost-effective ultra-high performance concrete, Mater. Struct. 50 (1) (2017) 29.
   [33] S. El-Tawil, Y.-S. Tai, B. Meng, W. Hansen, Z. Liu, Commercial production of non-
- [33] S. El-Tawil, Y.-S. Tai, B. Meng, W. Hansen, Z. Liu, Commercial production of non proprietary ultra high performance concrete, Michigan Department of Transportation Research Administration, 2018.

- [34] L.A. Sbia, A. Peyvandi, J. Lu, S. Abideen, R.R. Weerasiri, A.M. Balachandra, P. Soroushian, Production methods for reliable construction of ultra-highperformance concrete (UHPC) structures, Mater. Struct. 50 (1) (2017) 1–19.
- [35] W. Meng, K.H. Khayat, Improving flexural performance of ultra-high-performance concrete by rheology control of suspending mortar, Compos. B Eng. 117 (2017) 26–34.
- [36] L.e. Teng, W. Meng, K.H. Khayat, Rheology control of ultra-high-performance concrete made with different fiber contents, Cem. Concr. Res. 138 (2020), 106222.
- [37] H. Soualhi, E.-H. Kadri, A. Bouvet, T.-T. Ngo, F. Cussigh, A.-S.-E. Belaidi, New model to estimate plastic viscosity of eco-friendly and conventional concrete, Constr. Build. Mater. 135 (2017) 323–334.
- [38] H. Huang, L.e. Teng, X. Gao, K.H. Khayat, F. Wang, Z. Liu, Use of saturated lightweight sand to improve the mechanical and microstructural properties of UHPC with fiber alignment, Cem. Concr. Compos. 129 (2022), 104513.
- [39] M. Berry, R. Scherr, K. Matteson, Feasibility of non-proprietary ultra-high performance concrete (UHPC) for use in highway bridges in Montana: phase II field application, Montana Department of Transportation, 2020.
- [40] F. Mendonca, M.A. El-Khier, G. Morcous, J. Hu, Feasibility Study of Development of Ultra-High Performance Concrete (UHPC) for Highway Bridge Applications in Nebraska, Nebraska Department of Transportation, 2020.
- [41] Subedi, D., Non-Proprietary UHPC for Anchorage of Large Diameter Column Bars in Grouted Ducts (Doctoral dissertation). 2019.
- [42] B. Cazacliu, N. Roquet, Concrete mixing kinetics by means of power measurement, Cem. Concr. Res. 39 (3) (2009) 182–194.
- [43] S.M. Iveson, J.D. Litster, K. Hapgood, B.J. Ennis, Nucleation, growth and breakage phenomena in agitated wet granulation processes: a review, Powder Technol. 117 (1–2) (2001) 3–39.
- [44] S.M. Ivson, P.A. Wauters, S. Forrest, J.D. Litster, G.M. Meesters, B. Scarlett, Growth regime map for liquid-bound granules: further development and experimental validation, Powder Technol. 117 (1–2) (2001) 83–97.
- [45] H.H. Wong, A.K. Kwan, Packing density of cementitious materials: part 1—measurement using a wet packing method, Mater. Struct. 41 (4) (2008) 689–701.
- [46] A. Kaveh, S. Mahjoubi, Design of multi-span steel box girder using lion pride optimization algorithm, Smart Struct. Syst. 20 (5) (2017) 607–618.
- [47] S. Mahjoubi, X. Tan, Y.i. Bao, Inverse analysis of strain distributions sensed by distributed fiber optic sensors subject to strain transfer, Mech. Syst. Sig. Process. 166 (2022), 108474.
- [48] ASTM C230, Standard Specification for Flow Table for Use in Tests of Hydraulic Cement, ASTM International, West Conshohocken, PA, 2021.
- [49] Specification and Guidelines for Self-Compacting Concrete. 2002, European Federation for Specialist Construction Chemicals and Concrete Systems.
- [50] ASTM C109, Standard Test Method for Compressive Strength of Hydraulic Cement Mortars. ASTM International. West Conshohocken. PA, 2021.
- [51] ASTM C1698–19, Standard Test Method for Autogenous Strain of Cement Paste and Mortar, ASTM International, West Conshohocken, PA, 2019.
- [52] ASTM C403 C403/C403M, Standard Test Method for Time of Setting of Concrete Mixtures by Penetration Resistance, ASTM International, West Conshohocken, PA, 2017.